



HAL
open science

Loss of VPS13C Function in Autosomal-Recessive Parkinsonism Causes Mitochondrial Dysfunction and Increases PINK1/Parkin-Dependent Mitophagy

Suzanne Lesage, Valérie Drouet, Elisa Majounie, Vincent Deramecourt, Maxime Jacoupy, Aude Nicolas, Florence Cormier-Dequaire, Sidi mohamed Hassoun, Claire Pujol, Sorana Ciura, et al.

► To cite this version:

Suzanne Lesage, Valérie Drouet, Elisa Majounie, Vincent Deramecourt, Maxime Jacoupy, et al.. Loss of VPS13C Function in Autosomal-Recessive Parkinsonism Causes Mitochondrial Dysfunction and Increases PINK1/Parkin-Dependent Mitophagy. *American Journal of Human Genetics*, 2016, 98 (3), pp.500-513. 10.1016/j.ajhg.2016.01.014 . hal-01289266

HAL Id: hal-01289266

<https://hal.sorbonne-universite.fr/hal-01289266>

Submitted on 16 Mar 2016

HAL is a multi-disciplinary open access archive for the deposit and dissemination of scientific research documents, whether they are published or not. The documents may come from teaching and research institutions in France or abroad, or from public or private research centers.

L'archive ouverte pluridisciplinaire **HAL**, est destinée au dépôt et à la diffusion de documents scientifiques de niveau recherche, publiés ou non, émanant des établissements d'enseignement et de recherche français ou étrangers, des laboratoires publics ou privés.

**Loss of VPS13C function in autosomal recessive
parkinsonism causes mitochondrial dysfunction and
increases PINK1/Parkin-dependent mitophagy**

Suzanne Lesage,^{1,4,25} Valérie Drouet,^{1,4,25} Elisa Majounie,^{5,25} Vincent Deramecourt,⁶ Maxime Jacoupy,^{1,4} Aude Nicolas,^{1,4} Florence Cormier-Dequaire,^{1,4,7} Sidi Mohamed Hassoun,^{1,4} Claire Pujol,^{1,4} Sorana Ciura,^{1,4} Zoi Erpapazoglou,^{1,4} Tatiana Usenko,^{1,4} Claude-Alain Maurage,⁶ Mourad Sahbatou,⁸ Stefan Liebau,⁹ Jinhui Ding,⁵ Basar Bilgic,¹⁰ Murat Emre,¹⁰ Nihan Erginel-Unaltuna,¹¹ Gamze Guven,¹¹ François Tison,¹² Christine Tranchant,¹³ Marie Vidailhet,^{1,4,14} Jean-Christophe Corvol,^{1,4,7} Paul Krack,¹⁵ Anne-Louise Leutenegger,^{16,17} Michael A. Nalls,⁵ Dena G. Hernandez,⁵ Peter Heutink,¹⁸ J. Raphael Gibbs,⁵ John Hardy,¹⁹ Nicholas W. Wood,¹⁹ Thomas Gasser,¹⁸ Alexandra Durr,^{1,4,20} Jean-François Deleuze,²¹ Meriem Tazir,²² Alain Destée,²³ Ebba Lohmann,^{10,24} Edor Kabashi,^{1,4} Andrew Singleton,⁵ Olga Corti,^{1,4*} Alexis Brice,^{1,4,20**} on behalf of the French Parkinson's disease genetics study group (PDG) and the International Parkinson's disease consortium (IPDGC)

¹Sorbonne Universités, UPMC Université Paris 6 UMR S 1127, 75013 Paris, France; ²Inserm U 1127, 75013 Paris, France; ³CNRS UMR 7225, 75013 Paris, France; ⁴Institut du Cerveau et de la Moelle épinière, ICM, 75013 Paris, France; ⁵Laboratory of Neurogenetics, National Institute on Aging, Bethesda, MD 20892, USA; ⁶University of Lille Nord de France, Department of Histology and Pathology, Lille University Hospital, 59000 Lille, France; ⁷Centre d'Investigation Clinique Pitié Neurosciences CIC-1422, 75013 Paris, France; ⁸Fondation Jean Dausset-CEPH, 75010 Paris, France; ⁹Institute of Neuroanatomy, Eberhard Karls University Tübingen, 72074 Tübingen, Germany; ¹⁰Behavioural Neurology and

Movement Disorders Unit, Department of Neurology, Istanbul Faculty of Medicine, Istanbul University, 34390 Istanbul, Turkey; ¹¹Istanbul University, Institute for Experimental Medicine, Department of Genetics, 34390 Istanbul, Turkey; ¹²Institut des Maladies Neurodégénératives, Université de Bordeaux et CHU de Bordeaux, 33000 Bordeaux France; ¹³Pôle Tête-Cou-CETD, Service de Neurologie, Hôpitaux Universitaires, 67000 Strasbourg, France; ¹⁴Pôle des Maladies du Système Nerveux, Fédération de Neurologie, Hôpital de la Salpêtrière, 75013 Paris; France; ¹⁵Neurology Department, CHU de Grenoble, Joseph Fourier University, and INSERM U836, 38000 Grenoble, France; ¹⁶Inserm U946, 75010 Paris, France; ¹⁷Université Paris Diderot, Institut Universitaire d'Hématologie, UMR946, 75010 Paris, France; ¹⁸Hertie Institute for Clinical Brain Research, University of Tübingen and DZNE, German Center for Neurodegenerative diseases, 72074 Tübingen, Germany; ¹⁹Departments of Molecular Neuroscience, UCL Institute of Neurology, London WC1N 3BG, UK; ²⁰AP-HP, Hôpital de la Salpêtrière, Department of Genetics and Cytogenetics, 75013 Paris, France; ²¹Commissariat à l'Énergie Atomique, Institut Génomique, Centre National de Génotypage, 91000 Evry, France; ²²Service de neurologie CHU Mustapha, 16000 Alger, Algérie; ²³Lille University, Inserm U837, Movement Disorders Unit, Lille University Hospital, 59000 Lille, France; ²⁴Department of Neurodegenerative Diseases, Hertie Institute for Clinical Brain Research, University of Tübingen, and DZNE, German Center for Neurodegenerative Diseases, 72076 Tübingen, Germany

²⁵These authors contributed equally to this work.

Correspondence: * olga.corti@upmc.fr, ** alexis.brice@upmc.fr

Number of references: 43

Number of figures: 6

Number of table: 1

Number of characters including spaces in the title: 137

Number of words in the abstract: 173

Number of words in the main text: 4,799

ABSTRACT

Autosomal recessive early-onset parkinsonism is clinically and genetically heterogeneous. The genetic causes of approximately 50% of autosomal recessive early-onset forms of Parkinson's disease (PD) remain to be elucidated. Homozygosity mapping and exome sequencing in 62 isolated individuals with early-onset parkinsonism and confirmed consanguinity followed by data mining in the exomes of 1,348 PD individuals identified, in three isolated cases, homozygous or compound heterozygous truncating mutations in the *vacuolar protein sorting 13C* gene (*VPS13C*). *VPS13C* mutations are associated with a distinct form of early-onset parkinsonism characterized by rapid and severe disease progression and early cognitive decline; the pathological features were striking and reminiscent of diffuse Lewy body disease. In cell models, *VPS13C* partly localized to the outer membrane of mitochondria. Silencing of *VPS13C* was associated with lower mitochondrial membrane potential, mitochondrial fragmentation, increased respiration rates, exacerbated PINK1/Parkin-dependent mitophagy and transcriptional upregulation of *PARK2* in response to mitochondrial damage. This work suggests that loss of function of *VPS13C* is a cause of autosomal recessive early-onset parkinsonism with a distinctive phenotype of rapid and severe progression.

1 **Introduction**

2 Parkinson's disease (PD [MIM 168600]) is a motor syndrome with variable combinations of
3 akinesia, rigidity and rest tremor responding to levodopa. It is caused by degeneration of the
4 dopaminergic neurons in the *substantia nigra pars compacta*, and is associated with Lewy
5 bodies, intraneuronal inclusions enriched in α -synuclein. In recent years, our understanding of
6 the pathophysiological mechanisms underlying molecular defects in familial forms of PD has
7 greatly advanced. Three genes have been conclusively associated with autosomal dominant
8 (AD) forms of PD (*SNCA* [MIM 163890], *LRRK2* [MIM 609007], and *VPS35* [MIM 601501],
9 and eight (*PARK2* [MIM 602544], *PINK1* [MIM 608309], *DJ-1* [MIM 602533], *ATP13A2*
10 [*MIM* 610513], *FBXO7* [MIM 605648], *PLA2G6* [MIM 603604], *SYNJ1* [MIM 604297], and
11 *DNAJC6* [MIM 608375]) with early-onset (EO) autosomal recessive (AR) forms.¹ EO AR
12 parkinsonism is clinically and genetically heterogeneous: mutations in *PARK2*, *PINK1* and
13 *DJ-1* cause phenotypes similar to idiopathic PD with good and prolonged response to
14 dopaminergic therapy. Other EO AR PD-associated genes cause more severe disease, a poor
15 response to levodopa and additional clinical signs, such as dystonia and cognitive
16 impairment.¹ Mutations in *PARK2* and *PINK1* are the most common cause of EO AR PD,
17 accounting for ~50% and 4% of familial cases in Europe, respectively.^{2,3} A significant
18 proportion of cases remain genetically unexplained.

19 EO AR PD is linked to mitochondrial dysfunction. The mitochondrial kinase PINK1 and the
20 E3 ubiquitin-protein ligase Parkin cooperate in mitochondrial quality control.⁴ They promote
21 the removal of dysfunctional mitochondria in a process termed mitophagy that may also
22 involve FBXO7.^{4,5} In addition, they play a role in a vesicular trafficking pathway targeting
23 damaged mitochondrial components to the lysosome.⁶ To identify additional PD-associated
24 genes involved in AR EO parkinsonism, we performed homozygosity mapping and exome
25 sequencing in consanguineous PD families and isolated individuals and used data mining in

1 the exomes of 1,348 unrelated PD individuals. Five truncating mutations in the *vacuolar*
2 *protein sorting 13C* gene (*VPS13C* [MIM 608879]) were identified in three unrelated PD
3 isolated individuals. We provide evidence that depletion of the VPS13C protein exacerbates
4 mitochondrial vulnerability to stress.

5

6 **Subjects and Methods**

7 **Participants**

8 *Gene discovery cohort*

9 We selected nine PD families (with \geq two affected siblings) and 43 unrelated isolated
10 individuals according to the following criteria: 1) individuals diagnosed by neurologists
11 according to the UK Parkinson's Disease Society Brain Bank (PDSBB) clinical diagnostic
12 criteria⁷ and onset \leq 55 years in at least one affected family member; 2) with no mutations in
13 known PD-associated genes; and 3) with confirmed consanguinity (inbreeding coefficient
14 $F \neq 0$ computed with the FEstim program⁸). Sixteen families or isolated subjects were
15 European, 16 North African, 19 Turkish and one Lebanese. A total of 66 PD affected
16 individuals (23 family members and 43 isolated subjects) and 39 unaffected relatives were
17 included for the genome-wide screen study. Sixty-two affected and 10 unaffected individuals
18 were subsequently selected for whole exome sequencing.

19

20 *Validation cohort*

21 Exome data were obtained from a series of 1,348 additional PD individuals (99% unrelated,
22 99% of European ancestry, 60% males, mean age at onset 41.7 ± 11.0 years), including 249
23 French PD probands (57% males, age at onset \leq 40 years, 50 individuals with atypical forms
24 of parkinsonism) recruited by the French network for the study of PD genetics (PDG), and
25 530 matched control subjects (95% of European ancestry, 65% males, mean age at

1 examination: 45.1 ± 10.7 years), from the International Parkinson Disease Genomics
2 Consortium (IPDGC).

3 Hundred Turkish control subjects without family history of PD (43% males, mean age at
4 examination: 60.4 ± 13.9 years) served to check for the absence of the identified variant in
5 family A originated from Turkey.

6 A flow diagram detailing the selection criteria of PD individuals and controls, and the
7 different experimental steps of the study is provided (Figure S1).

8

9 *Study Approval*

10 Informed consent was obtained from all participants, and the genetic studies were approved
11 by local ethics committees (INSERM, CCPPRB du Groupe Hospitalier Pitié-Salpêtrière, Paris,
12 France).

13

14 **Neuropathological assessment**

15 The autopsy of the affected individual II-1 in family B (Figure 1) was performed
16 approximately 36 h *post mortem*. Brain tissues were fixed for six weeks in 10% buffered
17 formalin, extensively sampled and processed as previously described⁹. Immunohistochemistry
18 was performed by a Ventana Benchmark automate. We used hematoxylin-eosin staining for
19 histopathology. For immunochemistry, the antibodies used were: anti-Tau (in-house AD2,¹⁰ 1
20 ng/mL), anti- β -amyloid (4G8, 1:1,000, Sigma, France), anti- α -synuclein (LB509, 1:500,
21 Abcam, France), anti-ubiquitin (1:1,000, Dako, France), anti-TDP-43 (1:500, Protein Tech,
22 France), and anti-glial fibrillary acid protein (GFAP, 1:20,000, Dako, France). The degree of
23 neuronal loss and the frequency of α -synuclein-immunoreactive and other inclusions were
24 determined semi-quantitatively by visual inspection, in comparison to brains of three aged-
25 matched controls (2 males and 1 female) from the Lille Neurobank collection.

1

2 **Molecular Studies**

3 *Whole Genome Homozygosity Linkage Mapping*

4 Genome-wide screens were performed on all available affected (n = 66) and unaffected (n =
5 39) individuals from the gene discovery cohort using the Illumina HumanCytoSNP-12 v2.1
6 DNA Analysis BeadChip microarrays that contain ~300,000 single nucleotide polymorphisms
7 (SNPs) and ~1,300 markers of common copy number variations (CNVs). Homozygosity
8 tracks (> 2 Mb) were visualized with the Homozygosity Detector module, and CNV with the
9 Illumina cnvPartition module. The inbreeding coefficients F were computed with the FEstim
10 program.⁸ Samples from individuals with confirmed consanguinity ($F \neq 0$) were subjected to
11 exome sequencing.

12

13 *Whole Exome Sequencing*

14 Exons from 62 affected (19 relatives and 43 isolated individuals) and 10 unaffected family
15 members from the gene discovery cohort, and all the 1,348 affected and 530 control
16 individuals from the validation cohort were captured using different exome enrichment kits
17 from fragmented genomic DNA and sequenced as indicated in Table S1. Ten-fold mean
18 sequencing depth was achieved in 96.4% and 88.8% of baited regions in PD individuals and
19 controls, respectively, thirty fold mean sequencing depth was achieved across ~75% of
20 targeted regions.

21 Human reference sequence UCSC hg19 was used for sequence alignment and variant calling
22 with the Burrows-Wheeler Aligner¹¹ and the Genome Analysis Toolkit.¹² PCR duplicates were
23 removed prior to variant calling using Picard software. Variants were annotated with
24 ANNOVAR software¹³ (exomes from validation cohort) or SnpEff and SnpSift programs
25 (exomes from gene discovery cohort). Data were analyzed with Ingenuity® Variant Analysis

1 (IVA) TM software from Ingenuity System. Effects on mRNA splicing by putative splice
2 variants (+/-5 base pairs around splice junctions according to IVA threshold) were analyzed
3 with Splice Site Finder, MaxEntScan, NNsplice, Genesplicer and Human Splicing Finder¹⁴⁻¹⁶
4 all included in Alamut v3 software. The human VPS13C protein and its closest homologs
5 were aligned with Alamut v3 software, computed by Ensembl and aligned with MUSCLE.
6 An in-house pipeline crossed the output data from IVA and Homozygosity Mapping to filter
7 and identify the variants of interest (Figure S2). These variants were visualized using the
8 Broad Institute Integrative Genomics Viewer (IGV) and verified by bidirectional Sanger
9 sequencing using primers designed with Primer3 (Table S2) on an ABI 3730 automated
10 sequencer (Life Technologies, Carlsbad, CA, USA). Sanger sequencing confirmed the
11 absence of mutations in origin-matched controls and determined the genetic status of
12 unaffected relatives. Mutation nomenclature follows Human Genome Variation Society
13 (HGVS) recommendations: the longest *VPS13C* transcript 2A cDNA nucleotides (“c.”) are
14 numbered from the adenine of the first ATG translation initiation codon as nucleotide +1
15 (GenBank reference sequence NM_020821.2).

16

17 *Splicing defect analysis by RT-PCR*

18 Keratinocytes from affected individual V-2 in family A or peripheral blood lymphocytes from
19 affected individual II-1 in family C (Figure 1) were used for splicing defects analyses. Hair
20 follicles were plucked under sterile conditions and cultured in flasks coated with MG (1:10,
21 Corning, Tewksbury, USA). Keratinocytes were grown on 20 mg/mL collagen IV (Sigma-
22 Aldrich, St. Louis, USA) -coated dishes containing EpiLife medium with the HKGS
23 supplement (Life Technologies, Carlsbad, USA). Total RNA extraction was carried out with
24 the RNeasy Kit (Qiagen, Hilden, Germany), according to the manufacture’s manual. RNA
25 (250 ng) was reverse-transcribed into cDNA using iScript reverse transcription supermix

1 (Bio-Rad). Primers are listed in Table S2. RT-PCR products were Sanger-sequenced directly
2 or after sub-cloning into the pJET1.2/blunt vector (Thermo Scientific).

3

4 **Studies in mammalian cells**

5 *Mammalian expression vectors, siRNAs, cell culture, and transfection*

6 COS-7 and HEK293T cells were grown in Dulbecco's Modified Eagle Medium + Glutamax
7 (Life Technologies) supplemented with 10% goat serum (Life Technologies) and 1%
8 Penicillin-Streptomycin (Life Technologies). Cells were plated, at 80% confluence, on glass
9 coverslips (Thermo Scientific) in 24-well cell plates for immunofluorescence, 6-well plates
10 for qPCR, 10 cm-Petri dishes for subcellular fractionation by differential centrifugation and
11 for the mitochondrion isolation kit, or 75 cm²-flasks for continuous sucrose gradient and
12 Percoll gradient purification. Cells were co-transfected with siRNAs (15 to 30 nM) and
13 expression vectors using Lipofectamine 2000 (Life Technologies), in an antibiotic free
14 medium, according to the manufacturer's instructions. The siRNA used were: Hs_VPS13C_5
15 and Hs_VPS13C_6 (siVPS13C, Qiagen); PINK1 stealth siRNAs (siPINK1, Invitrogen);
16 AllStars negative control siRNA (siControl, Qiagen). Their efficacy was controlled by
17 quantitative real-time RT-PCR (Figure 5F). The expression vectors were: pcDNA3-HA-
18 PARK2, pcDNA3-HA-PINK1, pcDNA3-HA¹⁷ and pEGFP-C1 (Life Technologies). Where
19 indicated, the cells were incubated with 10 μ M CCCP (Sigma).

20

21 *Subcellular fractionation, trypsin digestion assay and western blot analyses*

22 For sucrose density gradient confluent HEK293T cells from five 75 cm²-flasks were
23 harvested and disrupted with a Dounce homogenizer (80 manual strokes) in 10mM Tris-HCl
24 buffer, pH 7.6 containing 10% w/v sucrose, 10 mM ethylenediaminetetraacetic acid (EDTA),
25 0.5 mM dithiothreitol (DTT), supplemented with protease and phosphatase inhibitors (0.2

1 mM sodium orthovanadate, 4 mg/ml sodium fluoride, 5.4 mg/ml β -glycerophosphate, and
2 Complete cocktail 1X – 11836145001, Roche). After three centrifugations at 600 x g for 5
3 min to remove cell debris, the cell lysate was layered on a 20-60% linear sucrose gradient in
4 Tris-HCl, pH 7.6, containing 10 mM EDTA, as previously described¹⁸. After 18 h of
5 centrifugation at 100,000 x g, successive 0.8 ml fractions were collected. Proteins were
6 precipitated on ice with 10 % trichloroacetic acid, pelleted by centrifugation at 13,000 x g for
7 45 min and resuspended in 100 μ l of loading buffer (Tris pH 6.8 60mM, SDS 4%, β -
8 mercaptoethanol 5%, glycerol and bromophenol blue).

9 Total protein fractions were obtained from cells lysed in 210 mM mannitol, 70 mM sucrose, 5
10 mM Tris pH 7.4, 0.2 mM EGTA, 0.1 mM EDTA, 0.5 mM DTT, 0.1% BSA and protease and
11 phosphatase inhibitors after centrifugation at 600 x g for 5 min at room temperature.

12 Mitochondrion-enriched fractions were obtained by differential centrifugation (HEK293T) or
13 magnetic isolation (COS-7) and digested with trypsin (Sigma), as previously described.^{17,19}

14 For isolation of pure mitochondria, cells were lysed in 250 mM mannitol, 5 mM HEPES pH
15 7.4, 5 mM EGTA with protease and phosphatase inhibitors and the crude mitochondrial
16 fraction was layered on top of a 30% Percoll gradient, as previously described.²⁰ Protein
17 concentrations were determined with Bio-Rad protein assays (Bio-Rad, 500-0006), based on
18 the Bradford method. Samples were boiled in protein sample buffer, resolved by SDS-PAGE,
19 transferred onto a nitrocellulose membrane (Protran, Whatman) and analyzed by western
20 blotting with selected primary and secondary antibodies (Table S3). Membranes were
21 incubated with enhanced chemiluminescence substrate (Pierce); chemiluminescent and
22 fluorescent signals were revealed on film (ECL, Amersham Hyperfilm) or captured with
23 Odyssey Imaging (Li-COR) systems and quantified with ImageJ software (NIH). Total or
24 cytoplasmic fractions were normalized to α -tubulin, mitochondrial fractions to PMPCB.
25 Three to six independent fractionation experiments were quantified.

1

2 *Analysis of mitochondrial respiration*

3 Cellular oxygen consumption was measured using high resolution respirometry
4 (OROBOROS Oxygraph-2k, Austria) in a temperature-regulated chamber at 37°C. Oxygen
5 consumption was measured in intact COS-7 cells at a density of 2.5×10^6 cells in 2 mL of
6 respiration assay medium (1x DMEM, GlutaMAX™, GIBCO) containing 4.5 g/L D-Glucose
7 and 4 mM L-glutamine, by sequential additions of 1 µg/mL oligomycin, 2.5 µM CCCP and 5
8 µM rotenone/10 µM antimycin A. We determined the following mitochondrial parameters:
9 *basal oxygen consumption* (= basal cellular respiration - non-mitochondrial respiration),
10 *proton leak* (= oligomycin-inhibited respiration - non-mitochondrial respiration), *maximal*
11 *respiratory capacity* (= maximal uncoupled respiration - non-mitochondrial respiration),
12 *reserve respiratory capacity* (= maximal uncoupled respiration - basal respiration), and *non-*
13 *mitochondrial respiration* (rotenone/antimycin A-inhibited respiration). Cells were then lysed
14 to quantify the protein content using the Bradford reagent, which was used to normalize the
15 oxygen consumption data. The results were expressed in pmol of O₂/s/mg of total protein.

16

17 *Immunostaining, $\Delta\Psi_{mt}$, respiration, mitochondrial morphology, and Parkin-dependent*
18 *mitophagy*

19 Immunocytochemical stainings were performed as described previously using the antibodies
20 and dilution conditions indicated in Table S3. Changes in $\Delta\Psi_{mt}$ were evaluated with the
21 potentiometric dye tetramethylrhodamine methyl ester (TMRM) as described in¹⁹.
22 Mitochondrial morphology was analyzed on COS-7 cells immunostained for the B subunit of
23 the mitochondrial processing peptidase (PMPCB) using an image-processing algorithm and
24 two descriptive parameters to assess mitochondrial length and branching: aspect ratio,
25 calculated as the ratio between major and minor axes of each mitochondrial object,

1 representing its length; and form factor, calculated as $\text{perimeter}^2/(4\pi \times \text{area})$, representing a
2 combined evaluation of the length and degree of branching of the mitochondrial network.^{21,22}
3 For Parkin-dependent mitophagy, cells were immunostained for PMPCB or the outer
4 mitochondrial membrane protein TOMM20 and quantified as described.¹⁷ Images were
5 acquired with an Olympus FV-1000 confocal microscope ($\times 60$ oil immersion objective, NA
6 1.35) and analyzed using ImageJ analysis software (NIH).

7

8 *Quantitative real-time RT-PCR*

9 To demonstrate the efficiency of the siRNA-mediated silencing of endogenous *VPS13C* in
10 HEK-293T cells, total RNA was isolated from cells transfected with control or *VPS13C* or
11 *PINK1* siRNA using the RNeasy plus Mini Kit (Qiagen) and QIAshredder (Qiagen). RNA
12 from each sample (500 ng) was reverse-transcribed into cDNA using iScript reverse
13 transcription supermix (Bio-Rad). Real-time PCR was performed with the LightCycler® 480
14 System (Roche Applied Science) and SsoAdvanced Universal SYBR Green Supermix (Bio-
15 Rad). Results were analyzed using LightCycler 480 sw 1.5 quantification Software (Roche
16 Applied Science). *Beta-actin* (ACTB) was used as the reference gene for normalization.
17 Primers are listed in Table S2.

18

19 **Statistical analysis**

20 Statistical significance was established at $p < 0.05$ and determined with an unpaired t-test in
21 Figures 4A (Aspect Ratio) and S6A, matched t-test in Figures 4C, 5B and 5D, Mann–
22 Whitney–Wilcoxon test in Figure 4A (Form Factor), one-way ANOVA in Figures 6 and S5,
23 or two-way ANOVA in Figures 4B, 5E and 5F.

24

25 **Results**

1 **Truncating mutations in *VPS13C* cause AR parkinsonism**

2 Genome-wide screens in an initial series of 66 affected and 39 unaffected subjects, using
3 DNA microarrays identified a mean of 16.3 regions of homozygosity ≥ 2 Mb on the 22
4 autosomes of each consanguineous individual (gene discovery cohort). No rare deleterious
5 large genomic rearrangements were detected. Exomes were subsequently sequenced in the 62
6 affected individuals with confirmed consanguinity (inbreeding coefficient $F \neq 0$) and 10
7 unaffected family members to identify homozygous variants which: 1) in priority, would
8 disrupt the protein function (frameshifts, stop codons or splicing variants); 2) were rare
9 [minor allele frequency (MAF) $< 1\%$] in dbSNP137, the National Heart Lung and Blood
10 Institute (NHBLI), Exome Sequencing Project (ESP) database, and the 1000 Genomes
11 Project; 3) were shared by affected siblings when available; 4) were heterozygous in parents
12 and/or heterozygous or wild-type in unaffected siblings when available; 5) fell within
13 homozygous intervals; and 6) were absent in the homozygous state from DNA of 530
14 controls. We identified rare or undescribed homozygous truncating variants within 32 genes,
15 each found in a single affected individual with consanguinity that fulfilled all these
16 prioritization criteria (Table S4). We screened these candidate genes for additional
17 homozygous or compound heterozygous mutations in a validation cohort. *VPS13C* (also
18 known as KIAA1421, NM_020821.2) on chr15q22 was mutated in a consanguineous Turkish
19 PD individual (V-2 in family A) from the gene discovery cohort, and in two additional French
20 PD isolated individuals (II.1 in family B, and II.1 in family C) from the validation cohort
21 (Figure 1A). In addition, we identified a total of 80 rare (MAF $< 1\%$ in public databases)
22 single heterozygous mostly nonsynonymous variants in *VPS13C* from the validation cohort,
23 including 14 present in at least one of the 530 European controls (Table S5). No additional
24 homozygous or compound heterozygous variants were found in the 31 other candidate genes.

1 The affected individual V-2 in family A harbored a homozygous splice-site mutation
2 c.8445+2T>G, intron 61 in *VPS13C* confirmed by Sanger sequencing; eight unaffected
3 relatives, including the mother, had heterozygous c.8445+2T>G mutations or wild-type
4 sequences (Figure 1A, Figure S3A). Affected individuals in families B and C were compound
5 heterozygotes (Figure 1A, Figures S3B and S3C): the affected individual II-1 in family B
6 with c.806_807insCAGA, exon 11 (p.Arg269Serfs*14) / c.9568G>T, exon 69 (p.Glu3190*)
7 variants; the affected individual II-1 in family C with c.4165G>C, exon 37 (p.Gly1389Arg) /
8 c.4777delC, exon 43 (p.Gln1593Lysfs*7) variants. Direct sequencing of *VPS13C* in the three
9 unaffected siblings (II-2, II-3, and II-4) in family B and the unaffected mother (I-1) in family
10 C showed that they all carried heterozygous mutations or wild-type alleles (Figure 1A, Figure
11 S3), indicating that all variations were located on different alleles. The five *VPS13C* variants
12 were absent in dbSNP137, 1000 Genomes Project, EVS (Table S6A) and Exome Aggregation
13 Consortium (ExAC) databases (Table S6B), and our European control exomes, except for the
14 missense p.Gly1389Arg variant found on one control chromosome. In addition, the
15 c.8445+2T>G mutation was absent from 200 Turkish control chromosomes. No disruptive bi-
16 allelic variants were found in our 530 control subjects; one disruptive homozygous variant
17 (rs199602573) was found in the EVS database and ExAC populations (1/6,246 and 2/61,547,
18 respectively), indicating that *VPS13C* homozygous disruptive variants are extremely rare in
19 non-PD populations (Tables S6 and S7).

20 The c.4165G>C and c.8445+2T>G mutations were predicted *in silico* to modify donor splice
21 sites, one base upstream and two bases downstream, respectively, of splice junctions (Figure
22 S4A). Reverse-transcription PCR analysis of potential splicing defects confirmed the
23 predictions (Figure S4B). RNA from the homozygous individual of family A showed at least
24 three shorter transcripts, lacking up to 231 nucleotides at the end of the exon 61. In the subject
25 with the heterozygous variant, shorter transcripts were barely visible, probably due to a high

1 instability of these aberrant RNAs. In family C, the longer transcript was found in the subject
2 with the heterozygous variant, containing 14 additional nucleotides from intron 37.
3 *VPS13C* contains 86 exons spanning a 208-kb genomic region and has two main transcript
4 variants, 1A (NM_017684.4) and 2A (NM_020821.2) (Figure 1B). While the transcript 1A,
5 lacking exons 6 and 7 and encoding a 3,710-amino acid protein, is expressed in most tissues,
6 including brain and peripheral blood cells, the longest transcript 2A encodes a brain-specific
7 3,753-amino acid protein.²³ Two additional isoforms with uncharacterized expression pattern
8 are reported in Ensembl (NM_018080.3 and NM_001018088.2) and lack the 4 last exons. All
9 the isoforms contain the splice site variants found in families A and C. *VPS13C* contains a
10 chorein domain at its N-terminus, a DUF1162 domain of unknown function and a putative
11 autophagy-related domain (Figure 1B). Except for the c.8445+2T>G variant, which is located
12 in the DUF1162 domain, none of the variants were found in the predicted domains.

13

14 **Clinical and pathological characteristics of affected individuals harboring *VPS13C*** 15 **mutations**

16 The three affected individuals harboring *VPS13C* mutations had early disease onset (25 to <
17 46 years) and typical parkinsonism (akineto-rigid syndrome, rest tremor, good levodopa
18 response). Disease progression, however, was particularly severe, with early cognitive
19 decline, loss of response to treatment, axial symptoms, and dysautonomia. Affected subjects
20 were bedridden within 15 years of clinical onset. Pyramidal signs and motor deficits were
21 observed in two affected individuals. Brain MRI was normal early in the disease, then
22 bilateral atrophy was observed in the frontal, parietal and temporal lobes (Table 1). Post-
23 mortem examination of the brain of the affected individual II-1 in family B, who died at age
24 49 of a bronchopneumopathy by gulp, showed mild frontal atrophy, including the primary
25 motor area (Figures 2A-2C). The pathology resembled diffuse Lewy body disease. Alpha-

1 synuclein and ubiquitin positive-Lewy bodies were observed in the brainstem, limbic system,
2 hippocampus and all cortical associative areas, including the parieto-occipital region (Figures
3 2D-2F, Table S8). Tau-immunoreactive neurofibrillary tangles and neurites were seen in the
4 brainstem, hippocampus and primary motor cortex (Figure 2G, Table S8). There were no
5 glial-, α -synuclein-, A β - or TDP-43-immunoreactive inclusions.

6

7 **Loss of *VPS13C* function affects mitochondrial morphology, transmembrane potential** 8 **and respiration**

9 To investigate the function of *VPS13C*, we explored its subcellular distribution in human
10 HEK293T by sucrose gradient fractionation (Figure 3A). *VPS13C* was enriched in the low-
11 density fractions 1 and 2 containing the early endosomal marker EEA1 and most of the
12 cytosolic protein Parkin. *VPS13C* was also found in higher density fractions containing
13 membrane and soluble markers of the Golgi apparatus (GOLGA2), the ER (Calnexin, BiP)
14 and mitochondria (TOMM70, PMPCB, PINK1). Here, it was most abundant in fractions 8-10,
15 containing the greatest proportion of TOMM70 and PMPCB. The mitochondrial localization
16 of *VPS13C* was confirmed in mitochondrion-enriched fractions and pure mitochondria from
17 HEK293T and COS-7 cells (Figures 3B and 3C). Limited trypsin digestion of mitochondrion-
18 enriched fractions caused concomitant loss of *VPS13C* and the outer mitochondrial
19 membrane receptor TOMM70 under conditions preserving the outer mitochondrial membrane
20 channel TOMM40 and mitochondrial matrix enzyme PMPCB, indicating that *VPS13C* is
21 located on the mitochondrial surface (Figure 3C).

22 We then investigated the impact of loss of *VPS13C* function on mitochondrial morphology,
23 transmembrane potential and respiration, reported to be affected in models of *PINK1* or
24 *PARK2* deficiency.^{24,25} The siRNA-mediated silencing of *VPS13C* in COS-7 cells reduced
25 *VPS13C* mRNA levels to no more than 25% of the control condition (Figure S6) and was

1 associated with perinuclear redistribution of mitochondria and mitochondrial fragmentation,
2 as confirmed by quantitative image analysis (Figure 4A). Evaluation of the mitochondrial
3 transmembrane potential ($\Delta\Psi_{mt}$) with the potentiometric dye tetramethylrhodamine methyl
4 ester (TMRM), revealed a significant decrease in the mean fluorescence intensity of
5 mitochondria in cells depleted of VPS13C (Figure 4B). The $\Delta\Psi_{mt}$ decrease was accompanied
6 by an increase in maximal respiration rates and respiratory reserve, as assessed by high
7 resolution respirometry in intact cells (Figure 4C). Similar results were obtained in HEK293T
8 cells (data not shown).

9

10 **Loss of VPS13C function exacerbates PINK1/Parkin-dependent responses to** 11 **mitochondrial depolarization**

12 We further investigated the relationship between *VPS13C* and *PINK1* and *PARK2*, both at the
13 transcript and protein levels, with respect to their well-characterized response to
14 mitochondrial damage. PINK1 accumulates on mitochondria and recruits Parkin to initiate
15 mitophagy in response to mitochondrial dysfunction.⁴ Mitochondrial depolarization, triggered
16 by the protonophore CCCP, partially redistributed VPS13C from mitochondria to the
17 cytoplasm without significantly changing *VPS13C* transcript levels (Figures 5A, 5B and 5F -
18 left panel); under these conditions PINK1 accumulated on mitochondria, as expected.⁴
19 *VPS13C* silencing did not affect PINK1 levels under basal conditions, but it exacerbated
20 CCCP-induced mitochondrial accumulation of PINK1 without impacting *PINK1* mRNA
21 abundance (Figures 5C, 5D and 5F - middle panel). Moreover, *VPS13C* silencing enhanced
22 mitochondrial translocation of Parkin triggered by CCCP (Figures 5C and 5E). It also
23 upregulated Parkin protein abundance in the cytosol without affecting *PARK2* transcript
24 levels at 3 h of CCCP treatment (Figure 5E and F - right panel). *PARK2* expression increases
25 in response to mitochondrial damage caused by mitochondrial toxins, including CCCP.^{26,27}

1 Here, *PARK2* transcript levels tended to be higher at 48 h of CCCP treatment (Figure 5F -
2 right panel). This response was significantly enhanced following silencing of *VPS13C* or
3 *PINK1*, suggesting greater mitochondrial damage. *PINK1* silencing was also associated with
4 down regulation of *VPS13C* transcript levels under basal conditions (Figure 5F - left panel),
5 an effect that was reversed by *PINK1* overproduction (Figure S5), indicating the existence of
6 multiple regulatory loops between *VPS13C*, *PARK2*, and *PINK1*. Consistent with the above
7 described effects on *PINK1* and Parkin, *VPS13C* silencing exacerbated *PINK1*/Parkin-
8 mediated mitophagy triggered by CCCP in COS-7 cells, a model that we previously validated
9 for the study of this process (Figures 6 and S6).^{17,19}

10

11 **Discussion**

12 This study establishes *VPS13C* mutations as a monogenic cause of EO AR parkinsonism.
13 Homozygous or compound heterozygous truncating mutations in three PD individuals, absent
14 from or present in the heterozygous state in available unaffected family members and in a
15 very large number of controls, strongly support the pathogenicity of *VPS13C* in EO
16 parkinsonism. We identified three affected individuals harboring *VPS13C* mutations and
17 could not perform co-segregation analyses, due to the lack of additional affected relatives in
18 the corresponding families. However, the affected individuals shared a specific, rare, and
19 extremely distinctive phenotype consisting of EO parkinsonism with very rapid progression
20 and dementia, which argues strongly for the pathogenicity of *VPS13C* mutations. The initial
21 phenotype, EO parkinsonism and a good response to levodopa treatment, is similar to that of
22 PD individuals with *PARK2*, *PINK1* or *DJ-1* mutations. However, the affected individuals
23 rapidly became bedridden because of the worsening of motor dysfunction and loss of
24 response to treatment. Dysautonomia and pyramidal signs were observed in two affected
25 individuals, also distinguishing the phenotype from the classical, slowly progressive EO PD.

1 The presence of numerous α -synuclein and ubiquitin-positive-Lewy bodies in the brainstem,
2 limbic system and many cortical areas was reminiscent of diffuse Lewy body disease,
3 consistent with a motor phenotype associated with dementia. α -synuclein Lewy bodies are
4 absent in most PD individuals with *PARK2* mutations,²⁸ but were observed in the single
5 autopsy case with *PINK1* mutations reported.²⁹ Tau-immunoreactive neurofibrillary tangles
6 and neurites were also observed in cases with *PARK2* mutations.²⁸ These features define
7 *VPS13C*-associated EO parkinsonism as a clinical, pathological and genetic entity belonging
8 to the group of synucleinopathies. In addition, our study also provides 31 potential candidate
9 genes harboring disruptive homozygous mutations in a single PD affected individual.
10 However, genetic replication and functional validation are still needed to confirm their
11 relevance to PD.

12 Alterations in other members of the *VPS13* family cause AR neurodegenerative disorders:
13 *VPS13A* (MIM 605978) (CHAC [MIM 200150]) is mutated in chorea-acanthocytosis
14 characterized by progressive neurodegeneration and red cell acanthocytosis;³⁰ *VPS13B* (MIM
15 607817) (COH1 [MIM 216550]) is mutated in Cohen syndrome characterized by
16 psychomotor retardation, microencephaly and eye abnormalities.³¹ *VPS13A*, *VPS13B*, and
17 *VPS13C* are also mutated in gastric and colorectal cancers with unstable microsatellites.³²
18 *VPS13C* belongs to a family of large *VPS13* proteins (*VPS13A-D*) similar to yeast *Vps13p*.²³
19 Like yeast *Vps*, mammalian vacuolar sorting proteins are crucial for vesicular transport.³³
20 Initial studies linked yeast *VPS13* orthologs to the delivery of proteins to the vacuole, the
21 mammalian lysosome equivalent.³⁴ Mutations in *VPS35*, encoding a core component of the
22 retromer complex regulating endosomal protein sorting, are implicated in AD late-onset
23 PD.^{35,36} *VPS35* is also involved in protein trafficking from mitochondria to peroxisomes
24 through mitochondria-derived vesicles.³⁷ *PINK1* and *Parkin* play a role in this transport route,
25 which delivers damaged mitochondrial cargo directly to lysosomes in response to

1 mitochondrial stress.⁶ However, the machinery regulating cargo selection and sorting into
2 vesicles remains to be identified. VPS13C may be involved in this process. Such a mechanism
3 would be consistent with its mitochondrial localization and the observed relocation to the
4 cytosol in response to mitochondrial damage.

5 Several other observations in mammalian cells suggest that, like PINK1 and Parkin, VPS13C
6 plays a role in mitochondrial maintenance. VPS13C depletion led to reduction of $\Delta\Psi_{mt}$ and
7 mitochondrial fragmentation in cell lines. Moreover, it enhanced maximal respiration rates
8 suggesting compensatory adaptation aimed at preserving $\Delta\Psi_{mt}$ levels. In neuronal cells,
9 which produce ATP mainly through mitochondrial oxidative phosphorylation and are unable
10 to switch to glycolysis under acute mitochondrial stress, such changes may in the long term
11 exacerbate generation of reactive oxygen species and trigger irreversible mitochondrial
12 damage.^{38,39} VPS13C depletion also upregulated PINK1/Parkin-dependent mitophagy and,
13 similarly to PINK1 depletion, it enhanced the previously reported transcriptional upregulation
14 of Parkin in response to toxin-induced mitochondrial dysfunction. Overall, these data suggest
15 that loss of *VPS13C* function increases mitochondrial vulnerability to stress and thereby
16 activates PINK1/Parkin-dependent mitochondrial quality control pathways. Based on the
17 inverse relationship between VPS13C and PINK1 protein levels on the mitochondrial surface,
18 we cannot exclude that VPS13C also acts as a negative regulator of PINK1.

19 Mitochondrial function is ensured by a series of interconnected finely orchestrated pathways,
20 activated in response to different degrees of mitochondrial dysfunction.⁴⁰ Excessive
21 mitophagy has been associated with α -synuclein-dependent neurodegeneration.⁴¹ Further
22 work is required to clarify the role of VPS13C in mitochondrial maintenance and dissect its
23 possible relation to PINK1/Parkin-dependent pathways.

24 Enrichment of VPS13C in cell fractions containing the early endosomal marker EEA1
25 suggests broader roles for VPS13C in vesicular trafficking. A more general involvement in

1 endosomal-lysosomal trafficking, possibly counteracting α -synuclein pathology as recently
2 reported for VPS35,⁴² might explain the diffuse α -synuclein pathology and rapid progression
3 to dementia in individuals with *VPS13C* mutations. Such a mechanism would potentially
4 represent a unifying link with cellular pathways involved in AD PD.

5 In summary, we describe truncating mutations in *VPS13C* associated with EO parkinsonism
6 with rapid progression and widely distributed Lewy bodies. A meta-analysis of PD genome-
7 wide association studies (GWAS) recently identified a susceptibility allele ~250 kb from the
8 *VPS13C* gene but not associated with either CpG methylation or mRNA expression,⁴³
9 suggesting that *VPS13C* can either cause a monogenic form of EO parkinsonism or confer
10 genetic susceptibility to PD. While we are confident that our work strongly implicates
11 *VPS13C* mutations in PD, further genetic studies in other populations are needed to confirm
12 their pathogenicity. The development of animal models in which *VPS13C* is stably inactivated
13 will help dissect the mechanisms by which loss of *VPS13C* function affects the survival of
14 dopaminergic neurons.

1 **Supplemental Data**

2 Supplemental Data include six figures and seven tables and can be found with this article
3 online at <http://>.

4

5 **Consortia**

6 Members of The French Parkinson's Disease Genetics Study (PDG) are Suzanne Lesage,
7 François Tison, Marie Vidailhet, Jean-Christophe Corvol, Yves Agid, Mathieu Anheim,
8 Anne-Marie Bonnet, Michel Borg, Emmanuel Broussolle, Philippe Damier, Alain Destée,
9 Alexandra Dürr, Franck Durif, Paul Krack, Stephan Klebe , Ebba Lohmann, Maria Martinez,
10 Pierre Pollak, Olivier Rascol, Christine Tranchant, Marc Vérin, François Viallet, and Alexis
11 Brice.

12 Members of The International Parkinson Disease Genomics Consortium (IPDGC) are
13 Suzanne Lesage, Elisa Majounie, François Tison, Marie Vidailhet, Jean Christophe Corvol,
14 Michael A. Nalls, Dena G. Hernandez, J. Raphael Gibbs, Alexandra Dürr, Sampath Arepalli,
15 Roger A. Barker, Yoav Ben-Shlomo, Daniela Berg, Francesco Bettella, Kailash Bhatia, Rob
16 M. A. de Bie, Alessandro Biffi, Bastiaan R. Bloem, Zoltan Bochdanovits, Michael Bonin,
17 Jose M. Bras, Kathrin Brockmann, Janet Brooks, David J. Burn, Gavin Charlesworth, Honglei
18 Chen, Patrick F. Chinnery, Sean Chong, Carl E. Clarke, Mark R. Cookson, Carl Counsell,
19 Philippe Damier, Jean-François Dartigues, Panos Deloukas, Günther Deuschl, David T.
20 Dexter, Karin D. van Dijk, Allissa Dillman, Jing Dong, Frank Durif, Sarah Edkins, Valentina
21 Escott-Price, Jonathan R Evans, Thomas Foltynie, Jianjun Gao, Michelle Gardner, Alison
22 Goate, Emma Gray, Rita Guerreiro, Clare Harris, Jacobus J. van Hilten, Albert Hofman,
23 Albert Hollenbeck, Peter Holmans, Janice Holton, Michèle Hu, Xuemei Huang, Heiko Huber,
24 Gavin Hudson, Sarah E. Hunt, Johanna Huttenlocher, Thomas Illig, Pálmi V Jónsson, Laura
25 L. Kilarski, Iris E. Jansen, Jean-Charles Lambert, Cordelia Langford, Andrew Lees, Peter

1 Lichtner, Patricia Limousin, Grisel Lopez, Delia Lorenz, Steven Lubbe, Codrin Lungu, María
2 Martinez, Walter Mätzler, Alisdair McNeill, Catriona Moorby, Matthew Moore, Karen E.
3 Morrison, Ese Mudanohwo, Sean S. O’Sullivan, Michael J. Owen, Justin Pearson, Joel S.
4 Perlmutter, Hjörvar Pétursson, Vincent Plagnol, Pierre Pollak, Bart Post, Simon Potter,
5 Bernard Ravina, Tamas Revesz, Olaf Riess, Fernando Rivadeneira, Patrizia Rizzu, Mina
6 Ryten, Mohamad Saad, Javier Simón-Sánchez, Stephen Sawcer, Anthony Schapira, Hans
7 Scheffer, Claudia Schulte, Manu Sharma, Karen Shaw, Una-Marie Sheerin, Ira Shoulson,
8 Joshua Shulman, Ellen Sidransky, Chris C. A. Spencer, Hreinn Stefánsson, Kári Stefánsson,
9 Joanna D. Stockton, Amy Strange, Kevin Talbot, Carlie M. Tanner, Avazeh Tashakkori-
10 Ghanbaria, Daniah Trabzuni, Bryan J Traynor, André G. Uitterlinden, Daan Velseboer,
11 Robert Walker, Bart van de Warrenburg, Mirdhu Wickremaratchi, Caroline H. Williams-
12 Gray, Sophie Winder-Rhodes, Isabel Wurster, Nigel Williams, Huw R. Morris, Peter Heutink,
13 John Hardy, Nicholas W. Wood, Thomas Gasser, Andrew B. Singleton, and Alexis Brice,

14

15 **Acknowledgments**

16 The authors are grateful to the families for their participation in this study. They thank Merle
17 Ruberg for critical reading of the manuscript, the DNA and Cell Bank of ICM, the Plate-
18 Forme d’Imagerie Cellulaire de la Pitié-Salpêtrière (PICPS), and Ebru Özer and Meltem Pak
19 for sample preparation. We are grateful to Lille brain bank for the gift of a brain ("Lille
20 Neurobank", BB-0033-00030). This study was supported by the National Research Funding
21 Agency (ANR-08-NEUR-004-01) in association with ERA-NET NEURON, the France-
22 Parkinson Association, the Roger de Spoelberch Foundation (R12123DD), the French
23 Academy of Sciences, the French program “Investissements d’avenir” (ANR-10-IAIHU-06)
24 and the European Joint Programme - Neurodegenerative Disease Research (JPND-
25 COURAGE-PD) project. This study was also supported by the Intramural Research Program

1 of the National Institute on Aging and the National Institutes of Neurological Disorders and
2 Stroke, National Institutes of Health, Department of Health and Human Services (project Z01
3 AG000958 and by MRC Grant G1100643/1), by the European Social Fund and by the
4 Ministry Of Science, Research and the Arts Baden-Württemberg. This work was also
5 supported by the Department of Defense, including grant 10064005/11348001, the French
6 Health Ministry (PHRC), France Parkinson Association, Lille University Hospital (A.D.), the
7 Atip/Avenir from the National Institute of Health and Medical Research (INSERM), the ANR
8 in association with the ERA-NET E-rare program, the France Alzheimer Association and a
9 Career Integration Grant from Marie Curie Actions (E.K.). C.P. received a postdoctoral
10 fellowship from the Cognacq-Jay Foundation. S.C. received a postdoctoral fellowships from
11 EMBO and AFM-Telethon.

12 We declare that we have no conflicts of interest for this study.

13

14 **Web Resources**

15 The URLs for data presented herein are as follows:

16

17 1000 Genomes Database, <http://www.1000genomes.org/>

18 ANNOVAR, <http://annovar.openbioinformatics.org/>

19 Broad Institute IGV, <https://www.broadinstitute.org/igv/>

20 BWA, <http://bio-bwa.sourceforge.net/>

21 dbSNP, <http://www.ncbi.nlm.nih.gov/projects/SNP/>

22 Ensembl, <http://www.ensembl.org/>

23 ExAC Browser, <http://exac.broadinstitute.org>

24 GATK, [http://www.acronymfinder.com/Genome-Analysis-Toolkit-\(software\)-\(GATK\).html](http://www.acronymfinder.com/Genome-Analysis-Toolkit-(software)-(GATK).html)

25 Human Splicing Finder (HSF), <http://www.umd.be/HSF3/HSF.html>

- 1 Ingenuity® Variant Analysis (IVA)™ software from Ingenuity System,
- 2 <http://www.ingenuity.com/variants>
- 3 MUSCLE, <http://www.ebi.ac.uk/Tools/msa/muscle/>
- 4 NCBI Gene, <http://www.ncbi.nlm.nih.gov/gene/>
- 5 NHBLI Exome Sequencing Project (ESP), Exome Variant Server,
- 6 <http://evs.gs.washington.edu/EVS/>
- 7 OMIM, <http://www.omim.org/>
- 8 Picard, <http://picard.sourceforge.net/>
- 9 Primer3, <http://www.bioinformatics.nl/cgi-bin/primer3plus/primer3plus.cgi>
- 10 SnpEff, <http://snpeff.sourceforge.net/>
- 11 SnpSift, <http://snpeff.sourceforge.net/SnpSift.html>
- 12 UCSC Genome Browser, <https://www.genome.ucsc.edu/>
- 13
- 14

1 References

- 2 1. Bonifati, V. (2014). Genetics of Parkinson's disease--state of the art, 2013. *Parkinsonism*
3 *Relat. Disord.* *20 Suppl 1*, S23–S28.
- 4 2. Lücking, C.B., Dürr, A., Bonifati, V., Vaughan, J., De Michele, G., Gasser, T., Harhangi,
5 B.S., Meco, G., Denèfle, P., Wood, N.W., et al. (2000). Association between Early-Onset
6 Parkinson's Disease and Mutations in the Parkin Gene. *N. Engl. J. Med.* *342*, 1560–1567.
- 7 3. Ibáñez, P., Lesage, S., Lohmann, E., Thobois, S., De Michele, G., Borg, M., Agid, Y.,
8 Dürr, A., Brice, A., and French Parkinson's Disease Genetics Study Group (2006). Mutational
9 analysis of the PINK1 gene in early-onset parkinsonism in Europe and North Africa. *Brain J.*
10 *Neurol.* *129*, 686–694.
- 11 4. Pickrell, A.M., and Youle, R.J. (2015). The Roles of PINK1, Parkin, and Mitochondrial
12 Fidelity in Parkinson's Disease. *Neuron* *85*, 257–273.
- 13 5. Burchell, V.S., Nelson, D.E., Sanchez-Martinez, A., Delgado-Camprubi, M., Ivatt, R.M.,
14 Pogson, J.H., Randle, S.J., Wray, S., Lewis, P.A., Houlden, H., et al. (2013). The Parkinson's
15 disease–linked proteins Fbxo7 and Parkin interact to mediate mitophagy. *Nat. Neurosci.* *16*,
16 1257–1265.
- 17 6. McLelland, G.-L., Soubannier, V., Chen, C.X., McBride, H.M., and Fon, E.A. (2014).
18 Parkin and PINK1 function in a vesicular trafficking pathway regulating mitochondrial
19 quality control. *EMBO J.* *33*, 282–295.
- 20 7. Hughes, A.J., Daniel, S.E., Kilford, L., and Lees, A.J. (1992). Accuracy of clinical
21 diagnosis of idiopathic Parkinson's disease: a clinico-pathological study of 100 cases. *J.*
22 *Neurol. Neurosurg. Psychiatry* *55*, 181–184.

- 1 8. Leutenegger, A.-L., Prum, B., Genin, E., Verny, C., Lemainque, A., Clerget-Darpoux, F.,
2 and Thompson, E.A. (2003). Estimation of the Inbreeding Coefficient through Use of
3 Genomic Data. *Am. J. Hum. Genet.* *73*, 516–523.
- 4 9. Buée-Scherrer, V., Condamines, O., Mourton-Gilles, C., Jakes, R., Goedert, M., Pau, B.,
5 and Delacourte, A. (1996). AD2, a phosphorylation-dependent monoclonal antibody directed
6 against tau proteins found in Alzheimer's disease. *Brain Res. Mol. Brain Res.* *39*, 79–88.
- 7 10. Deramecourt, V., Lebert, F., Maurage, C.-A., Fernandez-Gomez, F.-J., Dujardin, S.,
8 Colin, M., Sergeant, N., Buée-Scherrer, V., Clot, F., Ber, I.L., et al. (2012). Clinical,
9 Neuropathological, and Biochemical Characterization of the Novel Tau Mutation P332S. *J.*
10 *Alzheimers Dis.* *31*, 741–749.
- 11 11. Li, H., and Durbin, R. (2010). Fast and accurate long-read alignment with Burrows-
12 Wheeler transform. *Bioinformatics* *26*, 589–595.
- 13 12. McKenna, A., Hanna, M., Banks, E., Sivachenko, A., Cibulskis, K., Kernytzky, A.,
14 Garimella, K., Altshuler, D., Gabriel, S., Daly, M., et al. (2010). The Genome Analysis
15 Toolkit: A MapReduce framework for analyzing next-generation DNA sequencing data.
16 *Genome Res.* *20*, 1297–1303.
- 17 13. Wang, K., Li, M., and Hakonarson, H. (2010). ANNOVAR: functional annotation of
18 genetic variants from high-throughput sequencing data. *Nucleic Acids Res.* *38*, e164.
- 19 14. Crooks, G.E., Hon, G., Chandonia, J.-M., and Brenner, S.E. (2004). WebLogo: A
20 Sequence Logo Generator. *Genome Res.* *14*, 1188–1190.

- 1 15. Desmet, F.-O., Hamroun, D., Lalande, M., Collod-Beroud, G., Claustres, M., and Beroud,
2 C. (2009). Human Splicing Finder: an online bioinformatics tool to predict splicing signals.
3 *Nucleic Acids Res.* 37, e67.
- 4 16. Schneider, T.D., and Stephens, R.M. (1990). Sequence logos: a new way to display
5 consensus sequences. *Nucleic Acids Res.* 18, 6097–6100.
- 6 17. Bertolin, G., Ferrando-Miguel, R., Jacoupy, M., Traver, S., Grenier, K., Greene, A.W.,
7 Dauphin, A., Waharte, F., Bayot, A., Salamero, J., et al. (2013). The TOMM machinery is a
8 molecular switch in PINK1 and PARK2/PARKIN-dependent mitochondrial clearance.
9 *Autophagy* 9, 1801–1817.
- 10 18. Erpapazoglou, Z., Froissard, M., Nondier, I., Lesuisse, E., Haguenaer-Tsapis, R., and
11 Belgareh-Touzé, N. (2008). Substrate- and Ubiquitin-Dependent Trafficking of the Yeast
12 Siderophore Transporter Sit1. *Traffic* 9, 1372–1391.
- 13 19. Bertolin, G., Jacoupy, M., Traver, S., Ferrando-Miguel, R., Saint Georges, T., Grenier, K.,
14 Ardila-Osorio, H., Muriel, M.-P., Takahashi, H., Lees, A.J., et al. (2015). Parkin maintains
15 mitochondrial levels of the protective Parkinson's disease-related enzyme 17- β
16 hydroxysteroid dehydrogenase type 10. *Cell Death Differ.*
- 17 20. Wieckowski, M.R., Giorgi, C., Lebiedzinska, M., Duszynski, J., and Pinton, P. (2009).
18 Isolation of mitochondria-associated membranes and mitochondria from animal tissues and
19 cells. *Nat. Protoc.* 4, 1582–1590.
- 20 21. Koopman, W.J.H., Verkaart, S., Visch, H.-J., Westhuizen, F.H. van der, Murphy, M.P.,
21 Heuvel, L.W.P.J. van den, Smeitink, J.A.M., and Willems, P.H.G.M. (2005). Inhibition of
22 complex I of the electron transport chain causes O₂⁻-mediated mitochondrial outgrowth.
23 *Am. J. Physiol. - Cell Physiol.* 288, C1440–C1450.

- 1 22. Buhlman, L., Damiano, M., Bertolin, G., Ferrando-Miguel, R., Lombès, A., Brice, A., and
2 Corti, O. (2014). Functional interplay between Parkin and Drp1 in mitochondrial fission and
3 clearance. *Biochim. Biophys. Acta BBA - Mol. Cell Res.* *1843*, 2012–2026.
- 4 23. Velayos-Baeza, A., Vettori, A., Copley, R.R., Dobson-Stone, C., and Monaco, A.P.
5 (2004). Analysis of the human VPS13 gene family. *Genomics* *84*, 536–549.
- 6 24. Exner, N., Treske, B., Paquet, D., Holmström, K., Schiesling, C., Gispert, S., Carballo-
7 Carbajal, I., Berg, D., Hoepken, H.-H., Gasser, T., et al. (2007). Loss-of-function of human
8 PINK1 results in mitochondrial pathology and can be rescued by parkin. *J. Neurosci. Off. J.*
9 *Soc. Neurosci.* *27*, 12413–12418.
- 10 25. Mortiboys, H., Thomas, K.J., Koopman, W.J.H., Klaffke, S., Abou-Sleiman, P., Olpin, S.,
11 Wood, N.W., Willems, P.H.G.M., Smeitink, J.A.M., Cookson, M.R., et al. (2008).
12 Mitochondrial function and morphology are impaired in parkin-mutant fibroblasts. *Ann.*
13 *Neurol.* *64*, 555–565.
- 14 26. Henn, I.H., Bouman, L., Schlehe, J.S., Schlierf, A., Schramm, J.E., Wegener, E., Nakaso,
15 K., Culmsee, C., Berninger, B., Krappmann, D., et al. (2007). Parkin mediates
16 neuroprotection through activation of I κ B kinase/nuclear factor- κ B signaling. *J.*
17 *Neurosci. Off. J. Soc. Neurosci.* *27*, 1868–1878.
- 18 27. Bouman, L., Schlierf, A., Lutz, A.K., Shan, J., Deinlein, A., Kast, J., Galehdar, Z.,
19 Palmisano, V., Patenge, N., Berg, D., et al. (2011). Parkin is transcriptionally regulated by
20 ATF4: evidence for an interconnection between mitochondrial stress and ER stress. *Cell*
21 *Death Differ.* *18*, 769–782.

- 1 28. Doherty, K.M., Silveira-Moriyama, L., Parkkinen, L., Healy, D.G., Farrell, M., Mencacci,
2 N.E., Ahmed, Z., Brett, F.M., Hardy, J., Quinn, N., et al. (2013). Parkin Disease: A
3 Clinicopathologic Entity? *JAMA Neurol.* 70, 571–579.
- 4 29. Samaranch, L., Lorenzo-Betancor, O., Arbelo, J.M., Ferrer, I., Lorenzo, E., Irigoyen, J.,
5 Pastor, M.A., Marrero, C., Isla, C., Herrera-Henriquez, J., et al. (2010). PINK1-linked
6 parkinsonism is associated with Lewy body pathology. *Brain* 133, 1128–1142.
- 7 30. Rampoldi, L., Dobson-Stone, C., Rubio, J.P., Danek, A., Chalmers, R.M., Wood, N.W.,
8 Verellen, C., Ferrer, X., Malandrini, A., Fabrizi, G.M., et al. (2001). A conserved sorting-
9 associated protein is mutant in chorea-acanthocytosis. *Nat. Genet.* 28, 119–120.
- 10 31. Kolehmainen, J., Black, G.C.M., Saarinen, A., Chandler, K., Clayton-Smith, J., Traskelin,
11 A.-L., Perveen, R., Kivitie-Kallio, S., Norio, R., Warburg, M., et al. (2003). Cohen Syndrome
12 Is Caused by Mutations in a Novel Gene, COH1, Encoding a Transmembrane Protein with a
13 Presumed Role in Vesicle-Mediated Sorting and Intracellular Protein Transport. *Am. J. Hum.*
14 *Genet.* 72, 1359–1369.
- 15 32. An, C.H., Kim, Y.R., Kim, H.S., Kim, S.S., Yoo, N.J., and Lee, S.H. (2012). Frameshift
16 mutations of vacuolar protein sorting genes in gastric and colorectal cancers with
17 microsatellite instability. *Hum. Pathol.* 43, 40–47.
- 18 33. Richardson, S.C.W., Winistorfer, S.C., Poupon, V., Luzio, J.P., and Piper, R.C. (2004).
19 Mammalian Late Vacuole Protein Sorting Orthologues Participate in Early Endosomal Fusion
20 and Interact with the Cytoskeleton. *Mol. Biol. Cell* 15, 1197–1210.
- 21 34. Bankaitis, V.A., Johnson, L.M., and Emr, S.D. (1986). Isolation of yeast mutants
22 defective in protein targeting to the vacuole. *Proc. Natl. Acad. Sci. U. S. A.* 83, 9075–9079.

- 1 35. Vilarino-Guell, C., Wider, C., Ross, O.A., Dachsel, J.C., Kachergus, J.M., Lincoln, S.J.,
2 Soto-Ortolaza, A.I., Cobb, S.A., Wilhoite, G.J., Bacon, J.A., et al. (2011). VPS35 Mutations
3 in Parkinson Disease. *Am. J. Hum. Genet.* 89, 162–167.
- 4 36. Zimprich, A., Benet-Pages, A., Struhal, W., Graf, E., Eck, S.H., Offman, M.N.,
5 Haubenberger, D., Spielberger, S., Schulte, E.C., Lichtner, P., et al. (2011). A Mutation in
6 VPS35, Encoding a Subunit of the Retromer Complex, Causes Late-Onset Parkinson Disease.
7 *Am. J. Hum. Genet.* 89, 168–175.
- 8 37. Braschi, E., Goyon, V., Zunino, R., Mohanty, A., Xu, L., and McBride, H.M. (2010).
9 Vps35 Mediates Vesicle Transport between the Mitochondria and Peroxisomes. *Curr. Biol.*
10 20, 1310–1315.
- 11 38. Almeida, A., Almeida, J., Bolaños, J.P., and Moncada, S. (2001). Different responses of
12 astrocytes and neurons to nitric oxide: The role of glycolytically generated ATP in astrocyte
13 protection. *Proc. Natl. Acad. Sci.* 98, 15294–15299.
- 14 39. Almeida, A., Moncada, S., and Bolaños, J.P. (2004). Nitric oxide switches on glycolysis
15 through the AMP protein kinase and 6-phosphofructo-2-kinase pathway. *Nat. Cell Biol.* 6,
16 45–51.
- 17 40. Rugarli, E.I., and Langer, T. (2012). Mitochondrial quality control: a matter of life and
18 death for neurons. *EMBO J.* 31, 1336–1349.
- 19 41. Choubey, V., Safiulina, D., Vaarmann, A., Cagalinec, M., Wareski, P., Kuum, M.,
20 Zharkovsky, A., and Kaasik, A. (2011). Mutant A53T alpha-synuclein induces neuronal death
21 by increasing mitochondrial autophagy. *J. Biol. Chem.* 286, 10814–10824.

1 42. Dhungel, N., Eleuteri, S., Li, L.-B., Kramer, N.J., Chartron, J.W., Spencer, B., Kosberg,
2 K., Fields, J.A., Stafa, K., Adame, A., et al. (2015). Parkinson's Disease Genes VPS35 and
3 EIF4G1 Interact Genetically and Converge on α -Synuclein. *Neuron* 85, 76–87.

4 43. Nalls, M.A., Pankratz, N., Lill, C.M., Do, C.B., Hernandez, D.G., Saad, M., DeStefano,
5 A.L., Kara, E., Bras, J., Sharma, M., et al. (2014). Large-scale meta-analysis of genome-wide
6 association data identifies six new risk loci for Parkinson's disease. *Nat. Genet.* 46, 989–993.

7

1 **Figure legends**

2

3 **Figure 1. Identification of *VPS13C* mutations**

4 (A) Pedigrees of families with *VPS13C* mutations. Black symbols represent individuals with
5 PD, open symbols, those unaffected. Arrows point to probands who underwent whole exome
6 sequencing. AE: age at examination; AD: age at death; AO: age at onset.

7 (B) Schematic representation of *VPS13C* and its variations. *VPS13C* spans 208kb and
8 contains 86 exons encoding a 3753-amino acid protein with a chorein domain at its N-
9 terminus, a DUF1162 domain of unknown function and a putative autophagy-related domain.

10 The five variations found in the 3 probands are indicated. Numbers above the gene identify
11 the exons containing *VPS13C* variations. Alternative splicing a and b represent skipping of
12 exons 6+7, and exon 82 respectively. Transcripts 1A, NM_017684.4: splicing a + b; 2A,
13 NM_020821.2: splicing b; 1B, NM_018080.3: ends at exon 82; 2B, NM_001018088.2:
14 splicing a and ends at exon 82.

15

16 **Figure 2. Neuropathology in the proband of family B with c.806_807insCAGA /**
17 **c.9568G>T *VPS13C* mutations shows abundant α -synucleinopathy**

18 (A-C) Macroscopic appearance of the left hemisphere (fixed): lateral view (A); medial view
19 (B); coronal section at the level of the cerebral peduncle (C).

20 (D, E) Lewy bodies in pigmented neurons in the *substantia nigra* (D, arrow, hematoxylin-
21 eosin (HE) staining) and the parietal neocortex (E, arrowhead, HE staining).

22 (F) Representative image of α -synuclein-immunoreactivity in the frontal cortex showing
23 abundant Lewy bodies and neurites.

24 (G) Tau-immunoreactive neurofibrillary tangles in the primary motor cortex. Scale bars for
25 microscopic images: 50 μ m.

1

2 Figure 3. A pool of VPS13C is located on the outer mitochondrial membrane

3 (A) Sucrose gradient fractionation illustrating the subcellular distribution of the endogenous
4 VPS13C protein in HEK293T. Note the enrichment of the protein in fractions 1 to 3 and 8 to
5 10. Soluble endoplasmic reticulum (ER, BiP) and mitochondrial (PMPCB) markers in
6 fractions 1 and 2 reflect organelle damage during fractionation.

7 (B) Western blot showing VPS13C immunoreactivity in mitochondria purified by Percoll
8 gradient centrifugation from HEK293T cells (pM fraction). Note the enrichment in VPS13C
9 and the mitochondrial markers, TOMM70 and PMPCB, in the pM fraction compared to the
10 mitochondrion-enriched fraction (M). T: total lysate.

11 (C) Limited trypsin treatment of mitochondrion-enriched fractions (M) from HEK293T or
12 COS-7 cells caused loss of VPS13C and the mitochondrial surface marker TOMM70; the
13 outer mitochondrial membrane channel TOMM40 and the matrix marker PMPCB are
14 preserved.

15

**16 Figure 4. VPS13C silencing impacts mitochondrial morphology, transmembrane
17 potential and respiration**

18 (A) Representative immunofluorescence staining illustrating mitochondrial perinuclear
19 redistribution and fragmentation in COS-7 cells silenced for *VPS13C* (si*VPS13C*, 30 nM)
20 compared to cells treated with control siRNA (siControl, 30 nM): green, mitochondrial matrix
21 marker PMPCB; red, α -Tubulin. *VPS13C* silencing reduced *VPS13C* mRNA levels to no
22 more than 25% of the control condition (see Figure S6). Scale bar 10 μ m. Quantification of
23 Aspect Ratio and Form Factor (see Methods and ^{21,22}) shows reduced mitochondrial network
24 complexity in si*VPS13C* treated cells (means \pm SEM; **p < 0.01; ***p < 0.001, of n = 88 or
25 86 cells scored per condition).

1 (B) Analysis of the relative TMRM fluorescence of mitochondria in COS-7 cells transfected
2 as in (A), illustrating the decrease in $\Delta\Psi_{mt}$ in cells depleted for VPS13C. n = 40 cells per
3 condition from one experiment representative of three carried out. ***p < 0.001.

4 (C) Oxygen consumption rates in intact COS-7 cells transfected with siControl or siVPS13C.
5 The left panel shows the oxygen flux corrected for instrumental background from one
6 representative experiment. The graph in the right panel displays the respiration rates. Absence
7 of VPS13C is associated with increased maximal respiration (= maximal uncoupled
8 respiration under CCCP - non-mitochondrial respiration in the presence of the mitochondrial
9 complex I and III inhibitors, rotenone and antimycin A) and reserve capacity (= maximal
10 uncoupled respiration - basal respiration before the addition of the complex V inhibitor
11 oligomycin). Means \pm SEM; *p < 0.05, of 6 independent experiments.

12

13 **Figure 5. Loss of VPS13C function enhances mitochondrial accumulation of PINK1,**
14 **recruitment of Parkin and PARK2 upregulation in response to CCCP**

15 (A-B) Western blot (A) and (B) corresponding VPS13C protein levels (normalized to α -
16 Tubulin or PMPCB) in cytosolic (C), mitochondrion-enriched (M) and total (T) cell fractions
17 from HEK293T cells treated or not with CCCP (10 μ M, 3 h). VPS13C levels decreased
18 significantly in mitochondria following CCCP treatment, but tended to increase in cytosol
19 (means \pm SEM; *p < 0.05, of 6 independent fractionation experiments).

20 (C-E) Western blot (C) and (D, E) corresponding normalized protein levels in cytosolic and
21 mitochondrion-enriched fractions from HEK293T transfected with 30 nM of control siRNA
22 (siControl) or siRNA targeting VPS13C (siVPS13C). (D) CCCP treatment resulted in
23 accumulation of PINK1 (endogenous) in mitochondrion-enriched fractions (M) following
24 treatment with siControl (-) and, more significantly, with siVPS13C (+). (E) Accumulation of
25 Parkin (endogenous) on depolarized mitochondria was also strongly enhanced in cells treated

1 with si*VPS13C*. In addition, Parkin levels were upregulated in the cytosolic (C) fractions,
2 particularly in untreated cells (means \pm SEM; * $p < 0.05$ of 4 independent fractionation
3 experiments).

4 (F) Quantitative real-time RT-PCR showing relative mRNA levels, normalized to α -actin
5 (*ACTB*), in HEK293T cells treated with control siRNA (siControl), or siRNA targeting
6 *VPS13C* (si*VPS13C*) or *PINK1* (si*PINK1*), under basal conditions or following CCCP
7 treatment. Note the more than 30% decrease in *VPS13C* mRNA levels after *PINK1* silencing
8 under basal conditions, but not after CCCP treatment (left panel). Note also that *VPS13C* and
9 *PINK1* silencing enhance the upregulation of *PARK2* mRNA at 48 h of CCCP treatment (right
10 panel); means \pm SEM of 3-9 replicates per condition from 2 independent experiments (** $p <$
11 0.01; *** $p < 0.001$ compared to siControl within each condition of CCCP treatment; ### $p <$
12 0.001 between the indicated conditions of CCCP treatments).

13

14 **Figure 6. Loss of *VPS13C* function exacerbates *PINK1*/Parkin-dependent mitophagy**

15 (A) Immunofluorescence staining of a representative experiment illustrating *PINK1*/Parkin-
16 dependent mitophagy in COS-7 cells overproducing Parkin and silenced for *VPS13C* or
17 *PINK1* (20 nM siRNA) after CCCP treatment (10 μ M for 48 h): red, Parkin; green,
18 mitochondrial matrix marker PMPCB. Open arrows indicate loss of mitochondrial networks;
19 white arrows show preserved networks. Scale bar 10 μ m.

20 (B) Quantification of mitophagy in the conditions described in (A), expressed as the
21 proportion of COS-7 cells without PMPCB (black bars) or TOMM20 (grey bars) staining; the
22 si*VPS13C* treatment increased and si*PINK1* decreased the proportion. In the absence of
23 exogenous Parkin (- Parkin; cells overproducing the control protein EGFP) or CCCP (not
24 shown) all the cells harbored normal mitochondrial PMPCB staining, whether or not *VPS13C*

1 was silenced (means \pm SEM; *p < 0.05, **p < 0.01 of 3 independent experiments; 100 cells
2 scored per condition).

3 (C) Proportion of COS-7 cells without PMPCB staining after transfection with half-doses (10
4 nM) of each siRNA and 48 h of CCCP treatment. The mitophagy-promoting effect of
5 *VPS13C* depletion was abolished by concomitant silencing of *PINK1* (means \pm SEM; *p <
6 0.05 of 3 independent experiments; 100 cells scored per condition).

7

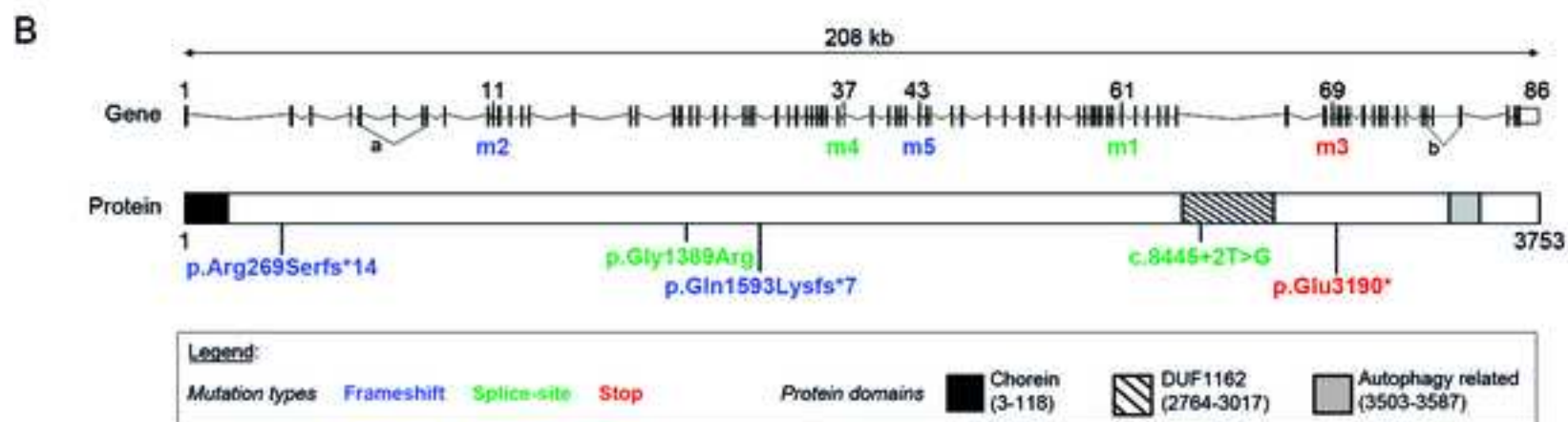
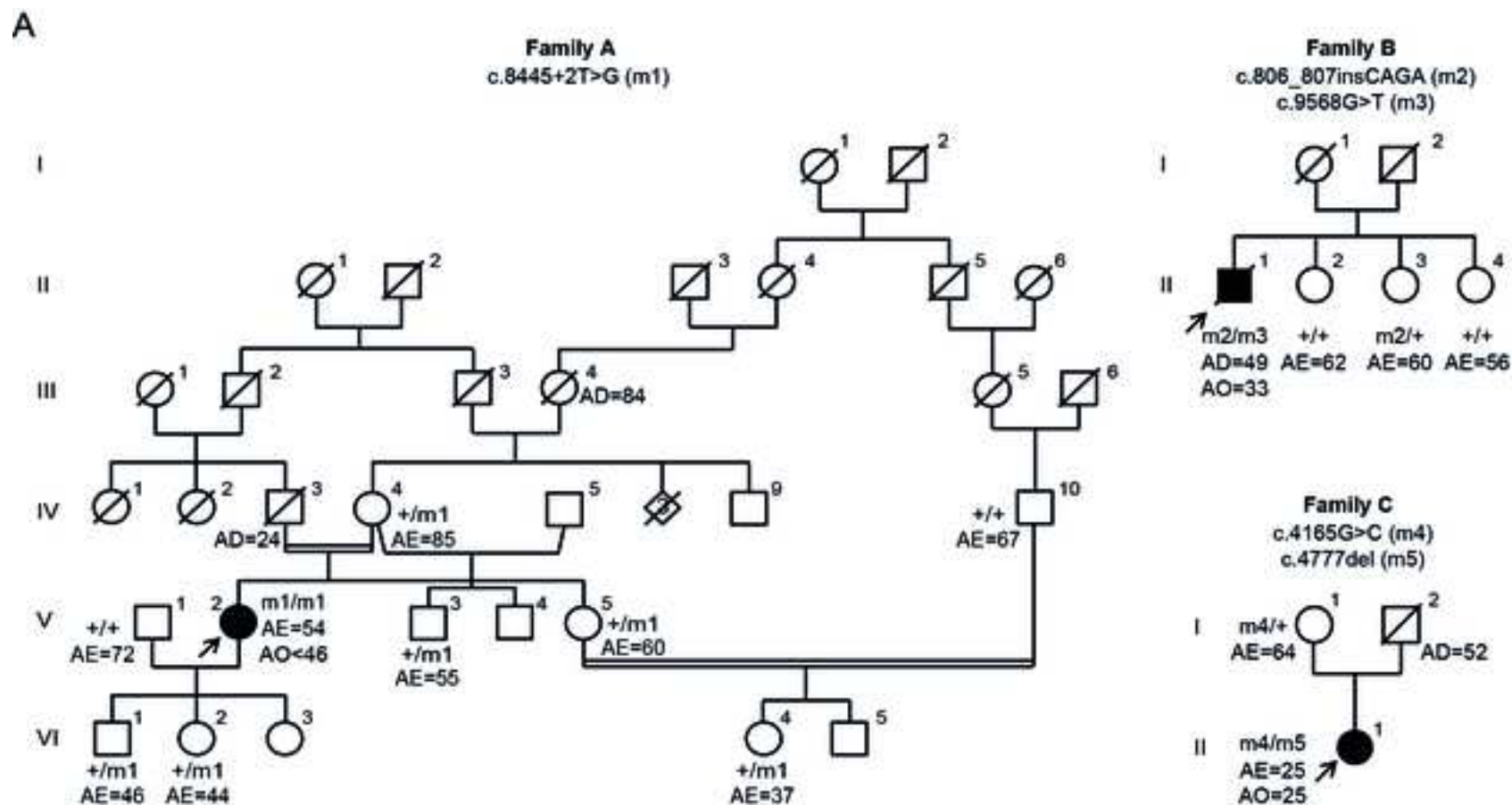
1 **Table 1. Clinical Characteristics of Affected Individuals Harboring *VPS13C* Mutations**

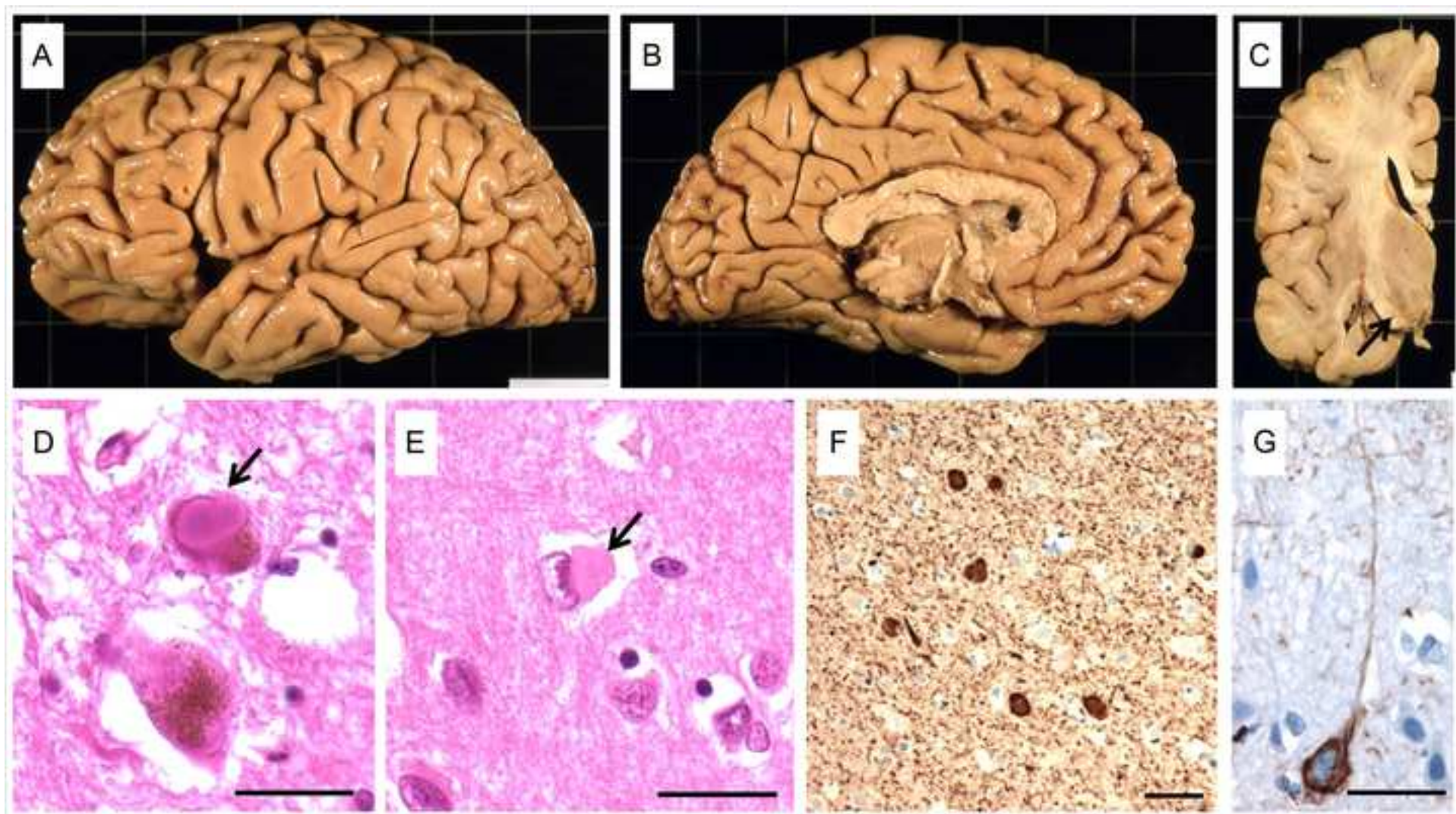
	V-2/family A	II-1/family B	II-1/family C
Origin	Turkish	French	French
Consanguinity	Yes	No	No
Gender	Female	Male	Female
Age at onset (years)	< 46	33	25
Symptoms at onset	Depression; Asymmetric akineto rigid syndrome; No dystonia	Asymmetric akineto rigid syndrome and rest tremor; Limb dystonia	Asymmetric akineto rigid syndrome; Limb dystonia
Response to levodopa	Yes, partial	Yes, at early stage	Yes, at early stage (evaluated at 75% initially)
Complications with treatment	No motor fluctuation nor dyskinesia	Fluctuation and dyskinesia, ICD, somnolence	No motor fluctuation nor dyskinesia
Evolution	Severe with early cognitive decline with spatial disorientation (MMSE 21), slurred speech and hallucinations at the age of 51; Axial symptoms	Severe with early cognitive decline (MMSE 18 at the age of 40); Axial symptoms (FOG at the age of 35, falls at the age of 39); Dysautonomia (at the	Severe with early cognitive decline, slurred speech before the age of 39; Severe axial symptoms at early stage; Bedridden at the age of 31;

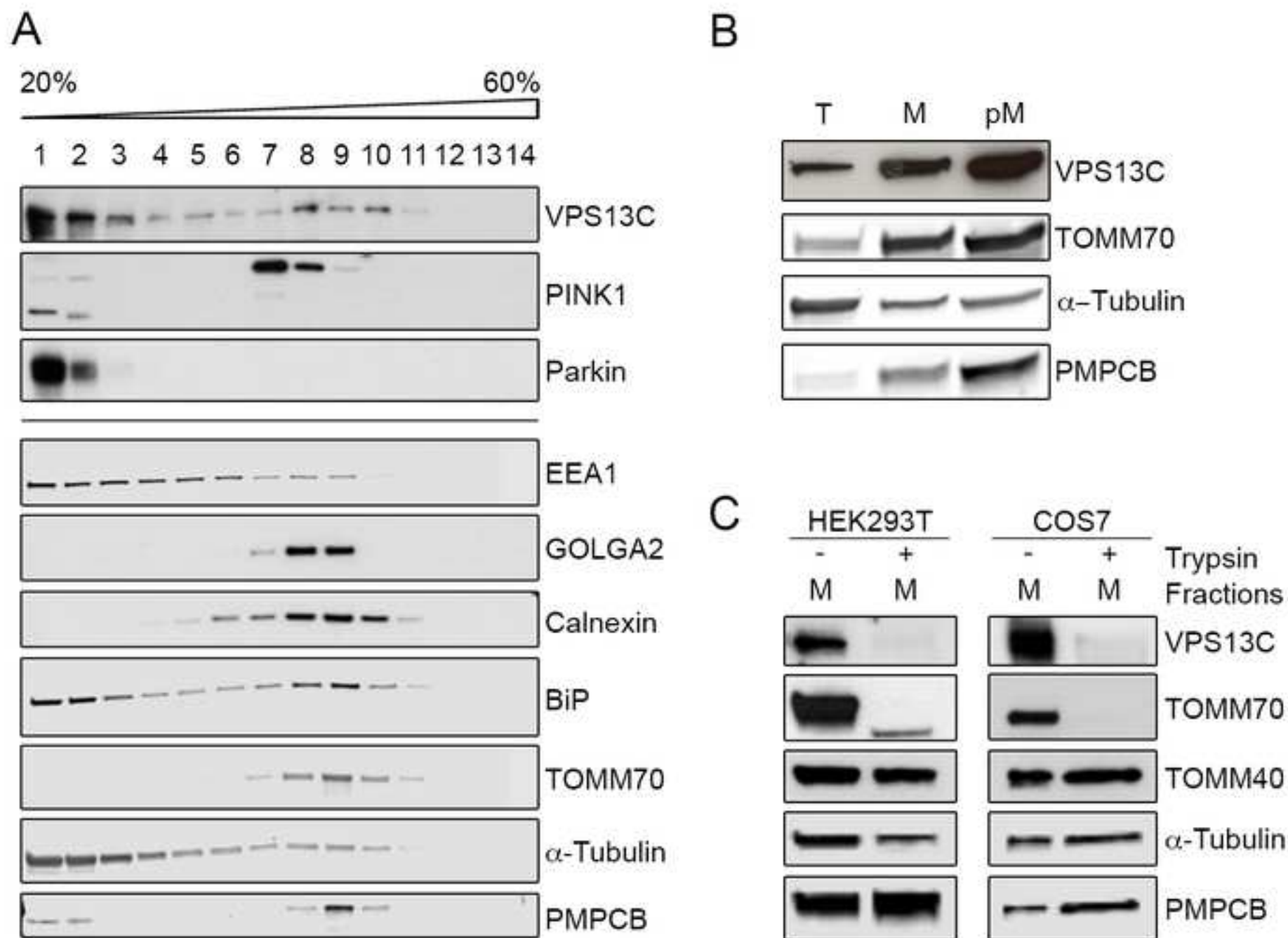
(postural instability, age of 35); Gastrostomia at the age
 FOG and falls) and Bedridden at the age of of 37
 dysautonomia with 43, death at the age of Her father died at 52 of
 urinary incontinence at 49 of a pancreatic cancer
 the age of 54; bronchopneumopathy
 Bedridden, unable to by gulp
 speak, apathetic,
 confused, cachexic with
 dysphagia at the age of
 58

Atypical symptoms associated	Brisk tendon reflexes on the lower limbs but no pyramidal syndrome	Motor neuron signs with pyramidal syndrome and limb atrophy at late stage	Motor neuron signs with spastic tetraplegia
Cerebral MRI	Asymmetric atrophy in frontal, parietal and temporal areas at the expense of the left side	Normal (performed at early stage)	Normal (performed at early stage)

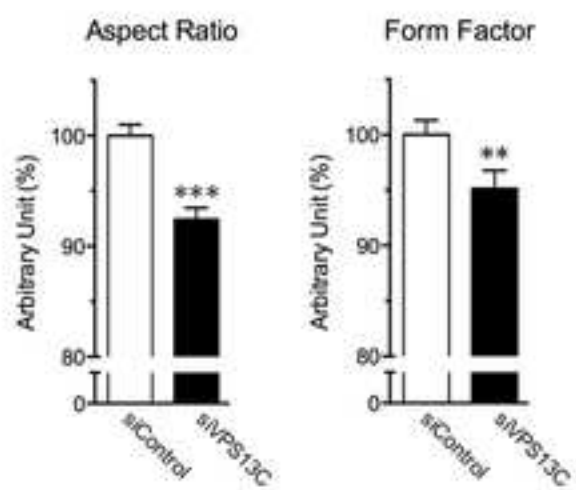
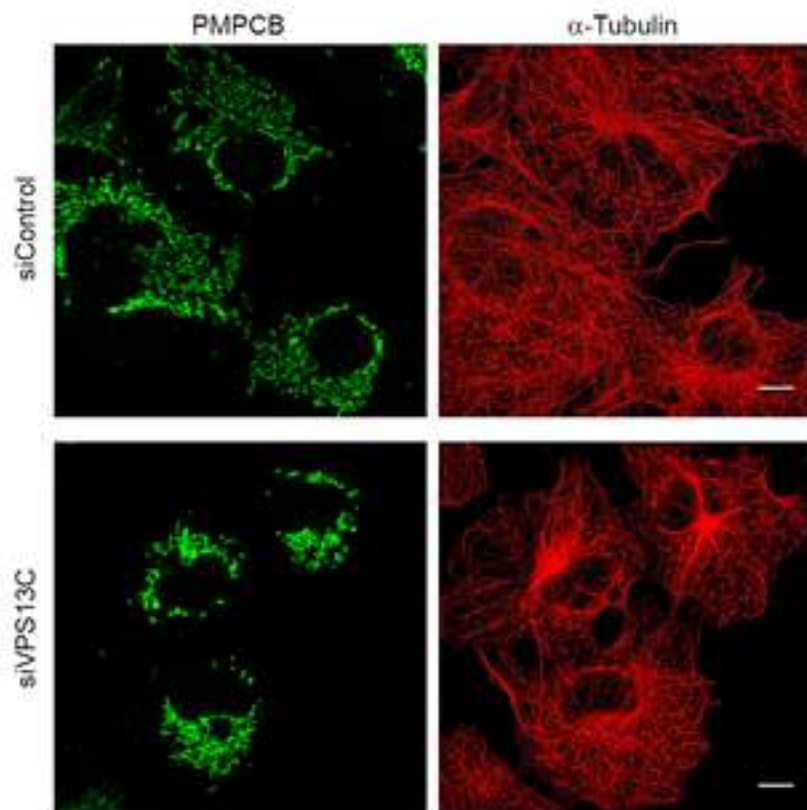
-
- 1 ICD, impulse control disorder; MMSE, mini-mental state examination; FOG, freezing of gait;
 - 2 MRI, magnetic resonance imaging.



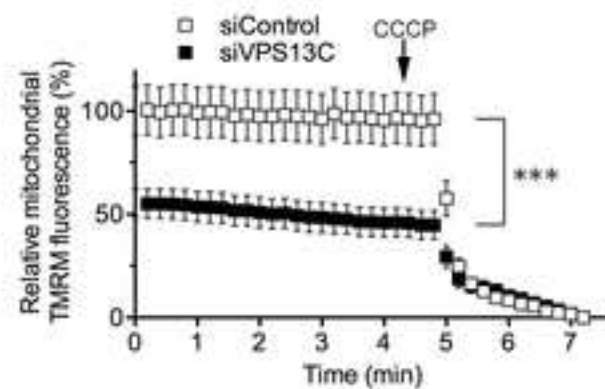




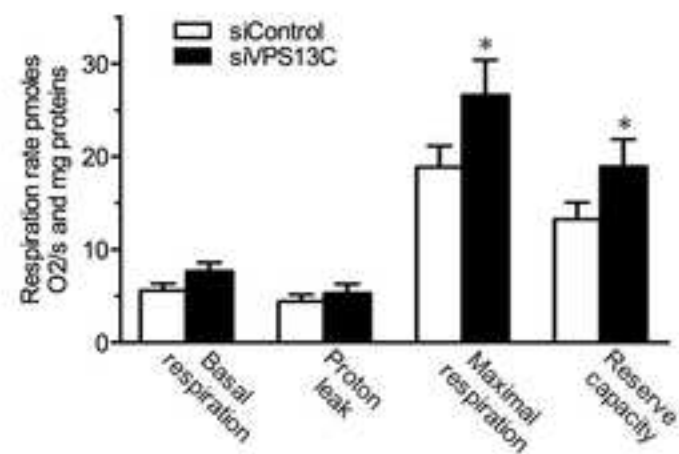
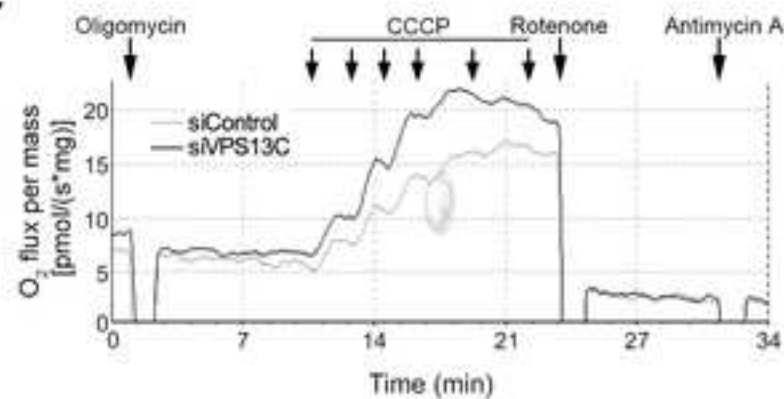
A

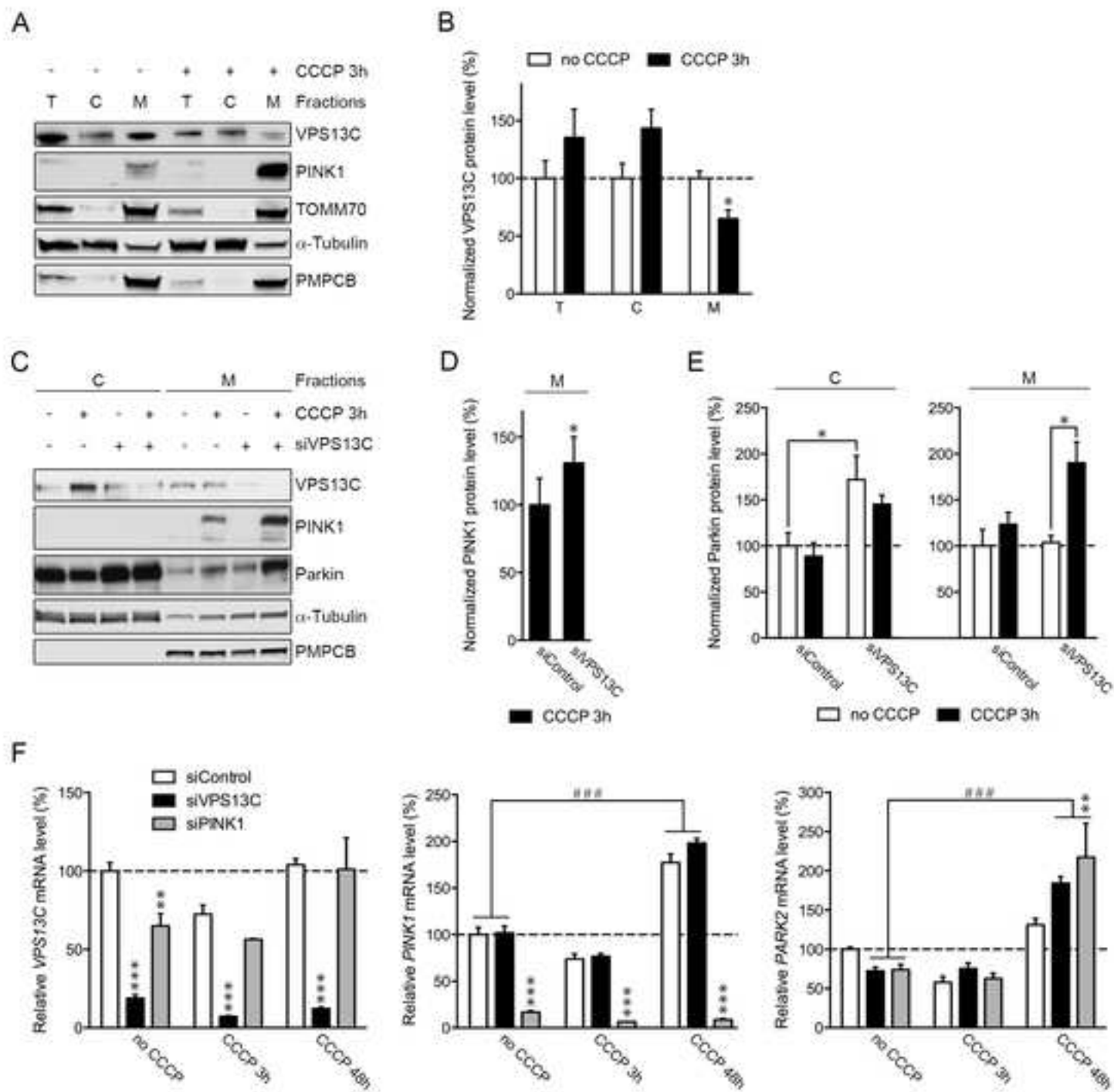


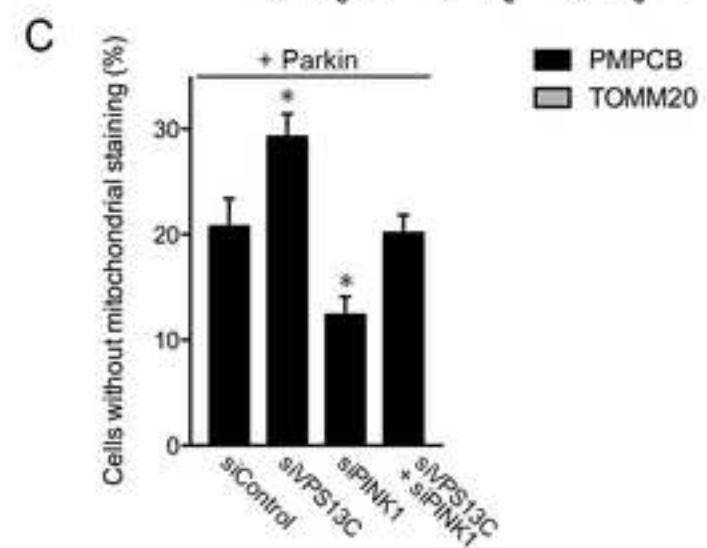
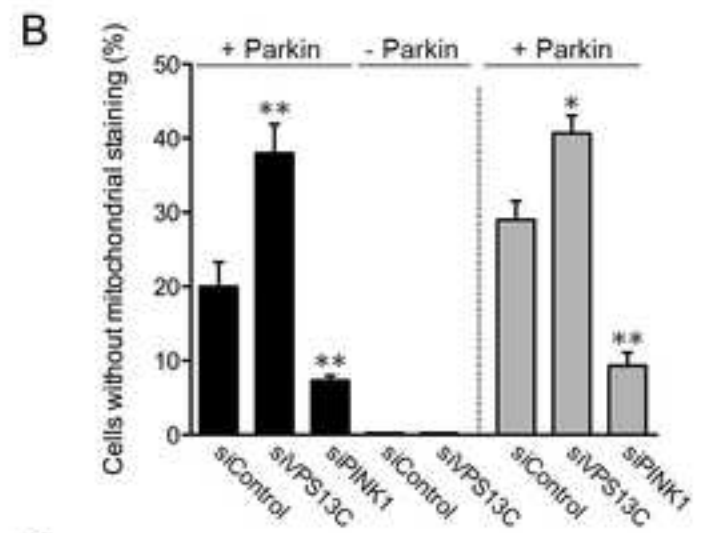
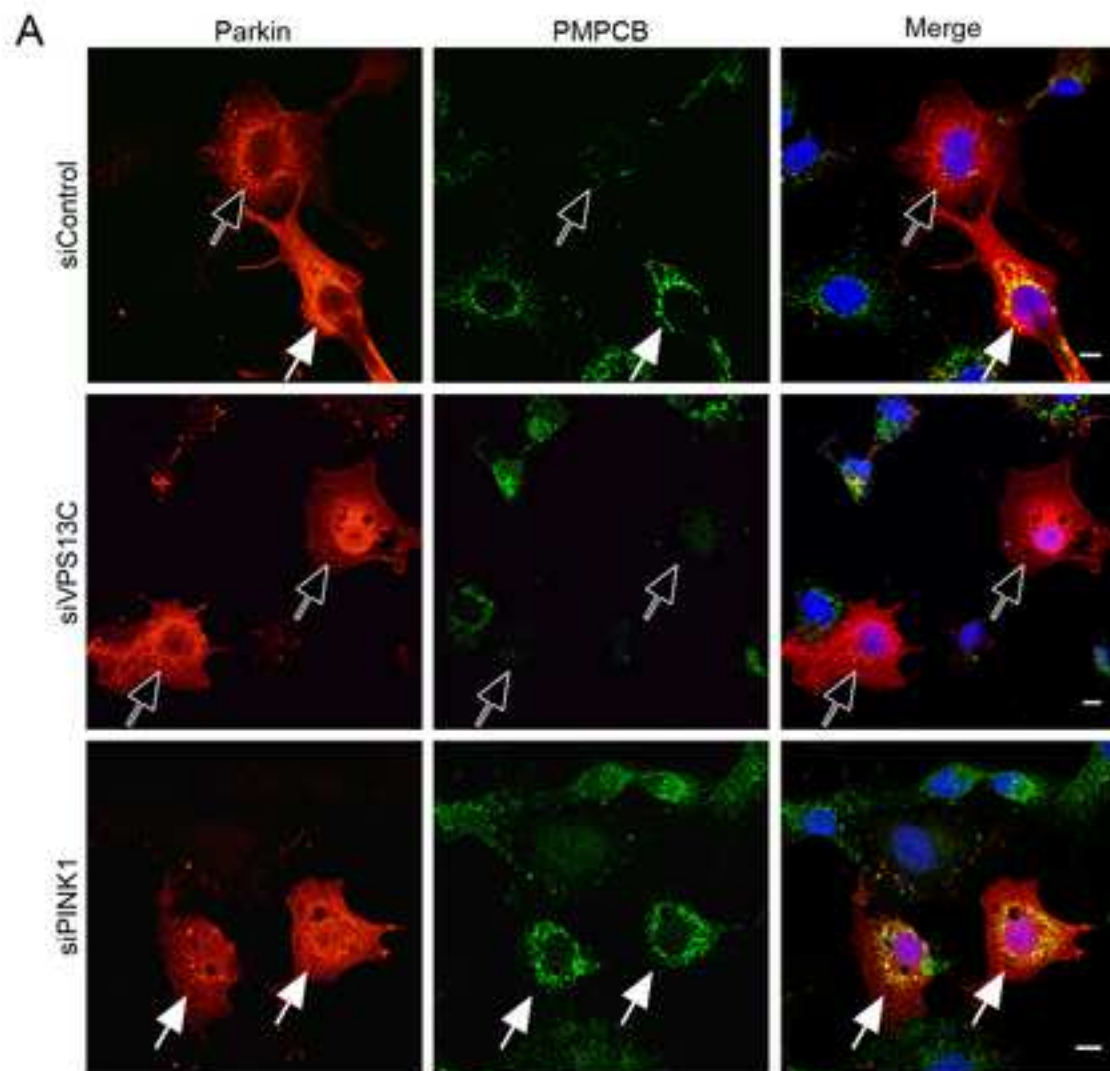
B

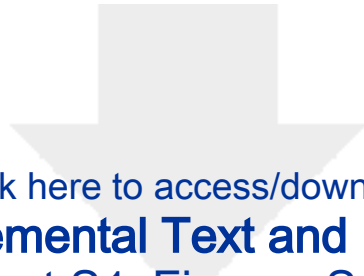


C



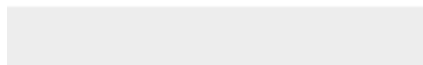






[Click here to access/download](#)

Supplemental Text and Figures
Document S1_Figures S1-S6.pdf





[Click here to access/download](#)

Supplemental Movies and Spreadsheets
Spreadsheets_Tables S1-S8.xlsx

